

Silencing cryptic specialized metabolism in *Streptomyces* by the nucleoid-associated protein Lsr2

Emma J. Gehrke^{1,2}, Xiafei Zhang^{1,2}, Sheila M. Pimentel-Elardo³, Andrew R. Johnson⁴, Christiaan A. Rees⁶, Stephanie E. Jones^{1,2}, Hindra^{1,2}, Sebastian S. Gehrke^{2,5}, Sonya Turvey^{1,2}, Suzanne Boursalie^{1,2}, Jane E. Hill⁶, Erin E. Carlson^{4,7}, Justin R. Nodwell³, Marie A. Elliot^{1,2*}

¹ Department of Biology and ² Michael G. DeGroot Institute for Infectious Disease Research, McMaster University, Hamilton, Ontario, Canada

³ Department of Biochemistry, University of Toronto, Toronto, Ontario, Canada

⁴ Department of Chemistry, Indiana University, Bloomington, Indiana, USA

⁵ Department of Biochemistry and Biomedical Sciences, McMaster University, Hamilton, Ontario Canada

⁶ Geisel School of Medicine and Thayer School of Engineering, Dartmouth College, Hanover, New Hampshire, USA

⁷ Department of Chemistry, University of Minnesota, Minneapolis, Minnesota, USA

Keywords: nucleoid-associated protein, *Streptomyces*, specialized metabolism, cryptic cluster, repression

* Corresponding author, E-mail: melliot@mcmaster.ca

1 ABSTRACT

2 Lsr2 is a nucleoid-associated protein conserved throughout the actinobacteria, including the antibiotic-
3 producing *Streptomyces*. *Streptomyces* species encode paralogous Lsr2 proteins (Lsr2 and Lsr2-like, or
4 LsrL), and we show here that of the two, Lsr2 has greater functional significance. We found that Lsr2
5 binds AT-rich sequences throughout the chromosome, and broadly represses gene expression.
6 Strikingly, specialized metabolic clusters were over-represented amongst its targets, and the cryptic
7 nature of many of these clusters appears to stem from Lsr2-mediated repression. Manipulating Lsr2
8 activity in model species and uncharacterized isolates resulted in the production of new metabolites not
9 seen in wild type strains. Our results suggest that the transcriptional silencing of biosynthetic clusters by
10 Lsr2 may protect *Streptomyces* from the inappropriate expression of specialized metabolites, and
11 provide global control over *Streptomyces*' arsenal of signalling and antagonistic compounds.

12

13 INTRODUCTION

14 Chromosomes are remarkably dynamic molecules. In eukaryotes, chromosome structure is
15 governed largely by histones, while in bacteria, organization is provided by the nucleoid-associated
16 proteins. Collectively, these proteins function both in architectural capacities and in regulatory roles.
17 Chromosome evolution in bacteria can be being driven by mutation, genome rearrangement, and
18 horizontal gene transfer, and work over the last decade has revealed that many bacteria have co-opted
19 nucleoid-associated proteins to additionally serve as 'genome sentinels', suppressing the inappropriate
20 expression of newly acquired DNA (Dorman, 2007; Dorman, 2014). This is thought to maximize
21 competitive fitness by repressing the expression of foreign DNA until it is either incorporated into the
22 existing regulatory networks of the host, or decays to a point that it is lost from the chromosome
23 (Navarre *et al.*, 2007).

24 Different bacteria employ distinct nucleoid-associated proteins as xenogeneic silencers,
25 including H-NS in the proteobacteria, MvaT/MvaU in the pseudomonads (Castang *et al.*, 2008), Rok in
26 *Bacillus* species (Smits and Grossman, 2010), and Lsr2 in the actinobacteria (Gordon *et al.*, 2008). None
27 of these proteins share sequence or structural homology, but all act by binding to AT-rich regions within
28 the chromosome (Navarre, 2006; Castang *et al.*, 2008; Gordon *et al.*, 2010; Smits and Grossman, 2010).
29 H-NS has been the best-studied of these proteins. In *Escherichia coli* and *Salmonella*, H-NS represses the
30 expression of pathogenicity islands, endogenous phage genes, as well as other genes needed to respond
31 to environmental changes (Lucchini *et al.*, 2006; Navarre, 2006). H-NS binds DNA as a dimer, and can

32 either polymerize along the DNA to form a rigid filament (Liu *et al.*, 2010), or bridge DNA to facilitate
33 chromosome compaction (Dame *et al.*, 2000; Dame *et al.*, 2006); both activities can limit the activity of
34 RNA polymerase. Lsr2 is thought to function similarly to H-NS. To date, its study has been confined to
35 the mycobacteria, where Lsr2 specifically binds and represses the expression of horizontally transferred
36 genomic islands and AT-rich regions, including major virulence factor-encoding genes (Gordon *et al.*,
37 2010).

38 In contrast to many of the pathogens in which chromosome organization and genome silencing
39 has been explored, the streptomycetes are largely benign, sporulating soil bacteria (Flårdh and Buttner,
40 2009) that are instead renowned for their ability to produce a wide array of specialized metabolites
41 (Hopwood, 2007; Barka *et al.*, 2016). Notably, the metabolic output of this actinobacterial genus
42 includes the majority of naturally-derived antibiotics used to treat bacterial infections. The
43 streptomycetes encode two Lsr2 paralogues, unlike their mycobacterial relatives who possess a single
44 *lsr2* gene. *Streptomyces* are additionally unusual in that they have linear chromosomes, where the
45 majority of the genes required for viability are clustered in the chromosome core, and more species-
46 specific and laterally-acquired genes are located in the flanking chromosome arms (Bentley *et al.*, 2002).
47 It is within these arm regions that most of the specialized metabolic clusters are found. Recent work has
48 revealed that specialized metabolic clusters are over-represented as horizontally-transferred elements
49 in the streptomycetes (McDonald and Currie, 2017), and that in the closely-related *Salinospora*, lateral
50 gene transfer is a major driver of specialized metabolism (Ziemert *et al.*, 2014).

51 Specialized metabolic gene clusters are subject to complex, hierarchical regulatory control (van
52 Wezel and McDowall, 2011; Liu *et al.*, 2013). Most *Streptomyces* clusters contain dedicated pathway-
53 specific regulators, which in turn are controlled by a suite of more globally-acting transcription factors.
54 Interestingly, however, most clusters are poorly expressed under normal laboratory conditions, and in
55 many cases their associated metabolites remain uncharacterized. This is also the case for the
56 filamentous fungi, many of whom have a broad, untapped specialized metabolic repertoire, courtesy of
57 transcriptional silencing by histones (Pfannenstiel and Keller, 2019). Significant efforts are being made to
58 stimulate the production of these ‘cryptic’ metabolites in both bacteria and fungi, as they are widely
59 regarded as productive sources of new natural products (Craney *et al.*, 2013; Ochi and Hosaka, 2013;
60 Scharf and Brakhage, 2013; Yoon and Nodwell, 2014; Daniel-Ivad *et al.*, 2017; Onaka, 2017).

61 We sought to investigate the role of the nucleoid-associated proteins Lsr2 and LsrL in gene
62 regulation in *Streptomyces*. We found that deleting *lsr2* from the chromosome of *Streptomyces*
63 *venezuelae* had minor effects on *S. venezuelae* growth and development and major effects on

64 metabolism. In contrast, deleting *lslL* had no detectable impact on development, and only a minor effect
65 on metabolism. Focussing on *Lsr2*, we determined that it bound AT-rich regions, generally repressed the
66 expression of prophage genes and other genes unique to *S. venezuelae* (presumably acquired by lateral
67 gene transfer), and suppressed antisense gene expression. The most profound effect of *lsl2* deletion,
68 however, was the large-scale activation of specialized metabolic cluster gene expression. *Lsr2* directly
69 repressed the transcription of many cryptic clusters in a way that is analogous to *Lsr2*- and H-NS-
70 mediated repression of pathogenicity islands in other bacteria, and histone-mediated cluster silencing in
71 fungi. Unexpectedly, *Lsr2* also controlled the expression of well-characterized and highly-conserved
72 clusters, suggesting that *Lsr2* control has been broadly integrated into the regulatory cascades governing
73 specialized metabolism. Our results suggest that *Lsr2* functions as a metabolic gatekeeper in the
74 streptomycetes, playing a critical role in the metabolic circuitry of these organisms, and that bacteria,
75 like fungi, employ chromosome structuring elements to control specialized metabolism. Finally, we have
76 manipulated *Lsr2* activity using dominant negative variants, and successfully promoted the production
77 of otherwise cryptic metabolites in a wide range of *Streptomyces* species.

78

79 RESULTS

80 ***Lsr2* and *Lsr2*-like (*LsrL*) in *Streptomyces venezuelae***

81 All *Streptomyces* species possess two *lsl2* homologues (Chandra and Chater, 2014). We
82 examined these gene products and found that within any given species, the homologues shared ~50%
83 end-to-end amino acid identity and 60-65% sequence similarity. One homologue shared both genomic
84 synteny and greater sequence similarity when compared with *Lsr2* from *M. tuberculosis* (**Figure S1**). We
85 termed this protein *Lsr2* (SVEN_3225 in *S. venezuelae*), and its more divergent homologue *LsrL*, for *Lsr2*-
86 like (SVEN_3832 in *S. venezuelae*).

87 To determine the biological role of these two genes and their products, we constructed single
88 and double mutants in *S. venezuelae*. Deleting *lsl2* had no observable effect on *S. venezuelae* growth in
89 liquid culture (**Figure 1A**). Sporulation was, however, reproducibly delayed in the mutant (**Figure 1A,B**),
90 and the ‘exploration’ capabilities of the mutant (Jones *et al.*, 2017) were altered compared with wild
91 type (**Figure S2**). Metabolism was also affected, with the mutant strain producing enhanced levels of
92 melanin compared with its wild type parent (**Figure 1B**). Melanin over-production and the delay in
93 sporulation could be partially complemented through the *in trans* expression of *lsl2* (**Figure S2**). In
94 contrast, deleting *lslL* had no discernable effect on *S. venezuelae* growth or development, while a
95 double *lsl2 lslL* mutant strain most closely resembled the *lsl2* single mutant (**Figure 1**).

96 We examined the expression of *Lsr2* and *LsrL* throughout the *S. venezuelae* life cycle using RNA
97 sequencing data collected at three time points, and found *Lsr2* transcripts reached maximal levels during
98 the later stages of liquid culture growth (**Figure 1C**). In comparison, *LsrL* levels were lower and peaked
99 earlier (**Figure 1C**). We focussed our subsequent investigations on *Lsr2*, given its higher transcript levels
100 and more pronounced mutant phenotype.

101 102 **Lsr2 represses the expression of horizontally acquired and specialized metabolic genes in *S.*** 103 ***venezuelae***

104 To begin understanding the effect of *Lsr2* on *Streptomyces* growth and metabolism, we isolated
105 RNA samples from wild type and *Lsr2* mutant strains (see above), and compared transcript levels for the
106 two strains using RNA-sequencing. The most striking differences were seen at the final growth stage
107 (third time point), coinciding with the timing of maximal *Lsr2* expression (**Figure 1C**). Using a stringent
108 cut-off (>4 fold change, with a *q* value <0.01), we found that 484 genes has significantly altered
109 expression in the *Lsr2* mutant relative to wild type (**Table S1**). This represented ~6% of genes in the
110 chromosome, and for the vast majority (>90%) of these genes, expression was up-regulated. These
111 differentially expressed genes included many horizontally acquired genes: ~10% were phage-related (43
112 of 484), and an additional 10% (47 genes) were unique to *S. venezuelae*, relative to the other
113 *Streptomyces* genomes available in StrepDB (strepdb.streptomyces.org.uk/) (**Figure 2A; Table S1**). We
114 also observed increased antisense expression in a number of instances, suggesting that like its H-NS
115 counterpart in *E. coli*, *Lsr2* can also suppress intragenic transcription (Singh *et al.*, 2014) (**Figure S3**).

116 We noted that *LsrL* expression was significantly increased relative to wild type (**Table S1**). There
117 was, however, no significant change in the expression of any of the well-characterized developmental
118 genes in the *Lsr2* mutant (**Table S1**). In contrast, specialized metabolic genes were disproportionately
119 affected by *Lsr2*, with 155 of 484 differentially impacted genes (**Table S1**) localized to specialized
120 metabolic clusters; this corresponded to ~15% of all predicted specialized metabolic genes in the
121 chromosome, compared with altered expression for <5% of all others (non-specialized metabolic genes).
122 Consistent with the enhanced brown pigmentation observed for the *Lsr2* mutant, we observed increased
123 expression for genes in one of the predicted melanin biosynthetic clusters (**Table 1; Table S1**). Overall,
124 deleting *Lsr2* led to altered expression for genes within 21 of 30 predicted or characterized specialized
125 metabolic clusters, with increased expression (ranging from 4~900×) observed for genes in 18 of these
126 clusters (**Table 1; Table S1**). Indeed, for six clusters, more than one-third of their genes were significantly
127 upregulated (**Table 1; Table S1**); predicted cluster boundaries are typically very generous (*e.g.* the

128 chloramphenicol cluster is predicted to extend from *sven_0902-0945*, while the experimentally
129 validated cluster encompasses *sven_0913-0928*), and as a result we anticipate that the relevant
130 proportion of upregulated genes in these clusters is actually much higher. Importantly, of these six
131 clusters, five were largely transcriptionally silent in the wild type strain (**Figure 3**), with an average RPKM
132 for the differentially affected genes being <10 in the wild type, compared with an average of >190 in the
133 *lsr2* mutant (**Table S1**).

134 We experimentally validated our RNA sequencing results using reverse transcription-PCR,
135 focussing on select genes from clusters specifying a range of predicted products (polyketides,
136 thiopeptides, butyrolactones, and non-ribosomal peptides). In each case, transcripts were only
137 reproducibly detected in the *lsr2* null mutant (**Figure S4**). This suggested that Lsr2 functions as a
138 principal regulator for the majority of specialized metabolites in *S. venezuelae*, repressing the activity of
139 these clusters under laboratory conditions.

140

141 **Lsr2 directly controls specialized metabolite cluster expression**

142 To determine whether the effects observed in our transcription profiling experiments stemmed
143 from direct or indirect control by Lsr2, we examined our RNA-seq data for significant changes in the
144 expression of any known global antibiotic regulators. Unexpectedly, none were affected by the loss of
145 Lsr2 (**Table S2**), suggesting that Lsr2 may directly impact specialized metabolic cluster expression. We
146 next conducted chromatin-immunoprecipitation (ChIP) sequencing experiments to identify Lsr2-
147 associated DNA sequences using a functional Lsr2-3×FLAG fusion-expressing strain (**Figure S2**). We
148 isolated immunoprecipitated DNA from FLAG-tagged and control (untagged Lsr2-expressing) strains late
149 during liquid culture growth, at a developmental stage corresponding to the third time point in our
150 transcriptional analyses. Using a stringent filter (q value <0.01), we identified 223 Lsr2 binding sites
151 distributed throughout the chromosome (**Figure 2A; Table S3**). These included sites within 17
152 specialized metabolic clusters (**Table 1**), with 14 of these clusters showing altered transcriptional profiles
153 in the *lsr2* mutant compared with the wild type strain (*e.g.* **Figure 3**).

154 The effect of Lsr2 on specialized metabolism, and the lack of association with other
155 characterized global regulators, collectively suggested that Lsr2 activity may represent a new level in the
156 regulatory cascades governing specialized metabolism. As most globally acting antibiotic regulators
157 exert their effects by controlling the expression of pathway-specific regulators (*e.g.* McKenzie and
158 Nodwell, 2007; Rigali *et al.*, 2008; Gao *et al.*, 2012; Wang *et al.*, 2013), we tested whether this was also
159 the case for Lsr2. For the 14 clusters that were bound directly by Lsr2 and had altered transcription

160 profiles, we examined where Lsr2 bound, relative to any potential cluster-specific regulators. For
161 approximately half (8 of 14), Lsr2 binding was associated with a regulatory gene (**Table 1**). For the
162 others, Lsr2 bound elsewhere in the cluster, suggesting an independent mechanism of regulation.

163

164 **Trends in Lsr2 binding and regulatory control**

165 To better understand how Lsr2 exerted its repressive effects, we undertook a more
166 comprehensive investigation into its binding and regulatory impacts. We first validated the specificity of
167 Lsr2 binding using electrophoretic mobility shift assays (EMSAs). We tested five ChIP-associated
168 sequences, and found that each of these effectively out-competed non-specific DNA probes for binding
169 by Lsr2. This indicated that Lsr2 preferentially bound the DNA regions identified in our ChIP assays
170 (**Figure S5**).

171 Our ChIP-seq results suggested that Lsr2 bound to 223 sites across the chromosome.
172 Interestingly, these sites were not concentrated in the arm regions where more of the species-specific
173 (and presumably laterally-acquired) sequences were located, but instead were enriched in the ‘core’
174 region of the chromosome (as defined by Bentley *et al.*, 2002) (**Figure 2B; Table S3**). When considering
175 all Lsr2 binding sites, ~25% of the associated genes (where Lsr2 bound immediately upstream and/or
176 overlapping with their coding sequences) had altered transcriptional profiles, and of these, more than
177 30% were in specialized metabolic clusters (19 of 63) (**Table 1; Table S3**)

178 We assessed whether there was any correlation between binding site position and regulatory
179 impact. We found that binding sites within the arm regions were more likely to have transcriptional
180 ramifications compared with those in the core [35% (left arm), 40% (right arm), 25% (core)] (**Figure 2B**).
181 Binding sites associated with transcriptional changes were also, on average, larger than those that had
182 no direct effect on transcription, at least for the left and core regions (**Table S3; Figure 2C**), although
183 there were a number of large sites within the core region that had no direct effect on transcription.

184 We next sought to understand whether there was any specificity to Lsr2 binding in the
185 chromosome. We analyzed the *in vitro*-confirmed Lsr2 binding sites (from **Figure S5**) using the MEME
186 server (Bailey *et al.*, 2009); however, no consensus motif could be identified. In examining the cluster-
187 associated binding sites more broadly, we found these sequences had an average GC-content of 62.9%.
188 When all Lsr2 binding sites were considered, an average GC-content of 65% was observed (**Table S3**),
189 well below the chromosome average of 72.4%.

190 Previous *in vitro* analyses of binding preferences for Lsr2 from *M. tuberculosis*, had defined an
191 eight nucleotide AT-rich sequence as being optimal (Gordon *et al.*, 2011). We analyzed both the S.

192 *venezuelae* genome, and our identified Lsr2 binding sites, for either AT-rich 20 nt segments ($\geq 50\%$ A/T),
193 or AT-rich 'core' sequences (defined as 5 of 6 consecutive nucleotides being A/T). To first determine the
194 relative AT density in the *S. venezuelae* chromosome, we assessed the number of 20 nt AT-rich stretches
195 in 30 randomly selected sequences – 15 that were 500 bp and 15 that were 1000 bp in length (**Dataset**
196 **S1**). We found that 7/15 of the shorter sequences lacked any AT-rich stretch (with the number of
197 stretches ranging from 0-20, with an average of 5), compared with 2/15 of the longer sequences (with
198 numbers ranging from 0-36, and an average of 10). In contrast, the vast majority (222/223) of Lsr2
199 target sequences possessed at least one AT-rich 20 nt stretch: shorter target sequences (≤ 500 bp)
200 contained anywhere from 0 to 27 non-overlapping stretches (average of 7), while longer sequences
201 (≥ 750 bp) contained between 8 and 291 (average of 64) (**Dataset S1**).

202 We next assessed the presence of AT-rich core sequences within both the random genome
203 sequences, and the Lsr2-bound sites (**Dataset S1**). For the random segments, 11/15 of the 500 bp
204 sequences lacked an AT-rich core (with numbers ranging from 0-10, with an average < 1). This closely
205 mirrored the absence of an AT-rich core in 10/15 of the 1000 bp sequences (range of 0-8, with an
206 average of 1.5). This is in stark contrast to the Lsr2 target binding sequences: only 9 of 223 target
207 sequences lacked an AT-rich core, with shorter sequences (≤ 500 bp) averaging three core sites (ranging
208 from 0-11), and larger sequences (≥ 750 bp) averaging 25 (ranging from 1-124). This collectively
209 suggested that while the presence of an AT-rich core sequence and multiple AT-rich segments may not
210 be sufficient to promote Lsr2 binding, they appear to be near universal characteristics of Lsr2-bound
211 sequences.

212 To experimentally assess the importance of these AT-rich sequences for Lsr2 binding, we
213 focussed our attention on the Lsr2 binding site located in the intergenic region between the divergently
214 expressed *sven_5106* and *sven_5107* genes within the predicted butyrolactone biosynthetic cluster
215 (**Table 1; Figure S6**). Using EMSAs, we compared Lsr2 binding to the wild type sequence (58% GC), with
216 binding to mutant sequences having increasing GC content (63%, 64% and 70%). Lsr2 bound the AT-rich
217 sequences with much higher affinity than the more GC-rich sequences, with very little binding observed
218 for the 70% GC-containing probe (**Figure S7**). Notably, there was little difference in binding seen for
219 sequences in which an AT-rich core was disrupted (64% GC), versus when the overall AT-content was
220 changed (63% GC) (**Figures S6 and S7**). To determine whether the Lsr2 preference for more AT-rich DNA
221 was also observed *in vivo*, we introduced these altered sequences in place of the wild type, within a
222 larger DNA fragment (spanning 9 kb and encompassing *sven_5105-07*) on an integrating plasmid vector,
223 and introduced these variants into the Lsr2-3 \times FLAG-expressing strain. We conducted ChIP experiments

224 for each strain, and quantified the amount of DNA specific for this region using quantitative PCR. We
225 observed far higher levels of the wild type sequence compared with any of the mutant sequences (>80%
226 less), presumably reflecting greater Lsr2 affinity for the wild type, AT-rich sequence (**Figure S7**). We also
227 assessed the expression of the flanking genes in each case, and observed little expression from the wild
228 type sequence, while increased expression was associated with the mutant sequences. This indicated
229 that decreased binding by Lsr2 led to increased transcription of the flanking genes (**Figure S7**).

230

231 **Lsr2 activity is not specific for newly acquired biosynthetic clusters**

232 Given that Lsr2 is predicted to be functionally equivalent to H-NS in *E. coli*, where H-NS inhibits
233 the expression of laterally-acquired DNA sequences, we wanted to determine whether Lsr2
234 preferentially bound and repressed the expression of recently acquired (poorly conserved) biosynthetic
235 clusters in *S. venezuelae*. To investigate cluster conservation, we subjected the sequence of each of the
236 30 *S. venezuelae* specialized metabolic clusters to BLAST searches. We focussed our attention on eight
237 phylogenetically divergent *Streptomyces* species, alongside three strains of *S. venezuelae*, and assessed
238 the conservation of each cluster within these streptomycetes (**Figure 4; Table 1**). As expected, we found
239 that Lsr2 bound and repressed the expression of genes in many poorly conserved/recently acquired
240 clusters. However, not all *S. venezuelae*-specific clusters were controlled by Lsr2, and several of the best
241 conserved clusters (*e.g.* siderophore/desferrioxamine-encoding biosynthetic cluster and bacteriocin-
242 encoding clusters) were under direct Lsr2 control (**Figure 4; Table 1**). This suggested that Lsr2 may
243 function both as a silencer of newly acquired clusters, and as a central regulator within the hierarchy
244 governing specialized metabolic cluster expression.

245

246 **Deleting Lsr2 reprograms specialized metabolism and yields novel compounds**

247 Given the abundance of specialized metabolic genes affected by Lsr2, we examined the
248 antibiotic production capabilities of the *lsr2* mutant. Crude methanol extracts from wild type and *lsr2*
249 mutant cultures were initially tested against the Gram-positive indicator bacterium *Micrococcus luteus*.
250 We observed a significant increase in growth inhibition for extracts from the *lsr2* mutant relative to the
251 wild type strain (**Figure 5A**). Using activity guided fractionation and purification coupled with LC/MS
252 analyses, we identified chloramphenicol as being the major inhibitory molecule (**Figure 5B**).
253 Chloramphenicol is a well-known antibiotic, but it is not expressed at appreciable levels by *S. venezuelae*
254 under normal laboratory conditions (**Figure 5B**) (Fernández-Martínez *et al.*, 2014).

255 We next compared the soluble metabolites produced by wild type and *lsr2* mutant strains, and
256 found each had a unique metabolic profile. We further tested the metabolic effects of deleting *lsrL*, and
257 *lsr2* in conjunction with *lsrL*, as the increased *lsrL* expression observed in the *lsr2* mutant suggested that
258 a double mutant may have more profound metabolic consequences than the *lsr2* mutation alone.
259 Comparing the metabolic profiles of these four strains revealed that the greatest effect stemmed from
260 the loss of *lsr2*, although the loss of *lsrL* (on its own, and in conjunction with *lsr2*) led to minor changes in
261 metabolic output (**Figure S8**). In comparing the production of individual metabolites in a wild type and
262 *lsr2* mutant strain, we first focussed our attention on compounds produced after 3 days of growth in
263 liquid MYM medium. We observed unique peaks in the *lsr2* mutant for venemycin, a chlorinated
264 venemycin derivative, as well as thiazostatin and watasemycin (**Figure 5C**). These compounds have all
265 been described recently; however, this is the first time they have been shown to be produced in *S.*
266 *venezuelae*, as their previous characterization required expression in a heterologous *Streptomyces* host
267 (Thanapipatsiri *et al.*, 2016; Inahashi *et al.*, 2017).

268 Further examination of the soluble metabolites of 3, 4 and 5 day cultures grown in MYM
269 medium yielded ESI(+) (electrospray ionization) metabolome profiles that were compared using XCMS, a
270 tool to identify, quantify, and compare metabolite profiles across samples (Smith *et al.*, 2006). While
271 there were a multitude of new and enriched metabolites produced by the *lsr2* mutant, we focussed our
272 attention on the most abundant compounds (intensities greater than 10^5). Within these highly abundant
273 metabolites, we identified six unique molecules produced only by the *lsr2* mutant (excluding isotopes,
274 adducts, chemical noise and irreproducible peaks across replicates). An additional five compounds were
275 significantly (>5×) more abundant in the *lsr2* mutant than wild type (**Table S4**). Of these new and
276 enhanced compounds, only one was a known molecule (ferrioxamine), produced by a well-conserved
277 cluster under *Lsr2* control (**Table 1**).

278 Included amongst the unique compounds was a novel peak of *m/z* 281 in the *lsr2* mutant (**Figure**
279 **5D**). Based on fragmentation analysis, this compound was predicted to be *N*-acetyl-7-chloro-L-
280 tryptophan. To determine the gene cluster responsible for producing this compound, we searched for
281 halogenase-encoding genes. We identified *sven_6229* as a reasonable candidate, as it was dramatically
282 (>200×) upregulated in an *lsr2* mutant (**Table S1**). It was also part of a large, otherwise transcriptionally
283 silent specialized metabolic gene cluster (the 'NRPS-ladderane' cluster in **Figure 3** and **Table 1**). We
284 mutated *sven_6229*, and found the *m/z* 281 peak disappeared (**Figure 5D**). A close homologue of
285 SVEN_6229, PrnA, catalyzes the conversion of L-tryptophan to 7-chloro-L-tryptophan (Dong *et al.*, 2005),
286 and mutant PrnA variants can yield 5-chloro-L-tryptophan (Lang *et al.*, 2011). We predicted that an

287 acetylated form of one of these two chlorinated tryptophan molecules most likely corresponded to the
288 novel m/z 281 molecule identified in the *lsr2* mutant. We synthesized the two analogues, and confirmed
289 the identity of the unknown compound as being *N*-acetyl-chlorotryptophan, by virtue of the near
290 identical MS/MS spectra of the synthetic candidates (**Figure S9**). Interestingly, however, co-elution
291 studies with the synthetic standards clearly demonstrated that the unknown species was neither the 5-
292 chloro, nor the 7-chloro isomer (**Figure S9**), suggesting that it is a new tryptophan-derived precursor.

293

294 **Lsr2 alters the volatile metabolome of *S. venezuelae***

295 *As S. venezuelae* also produces volatile compounds with important biological roles (Jones *et al.*,
296 2017), we compared the volatile molecules produced by wild type and *lsr2* mutant strains. After
297 eliminating peaks associated with the growth medium, 742 discrete peaks were detected for both
298 strains. Of these, 65 were reproducibly differentially expressed, with 38 being more abundant in the
299 wild type, and 27 more abundant in the *lsr2* mutant (**Figure 5E; Table S5**), suggesting that volatile
300 metabolites may not be subject to the same regulatory controls as other specialized metabolites.
301 Generally, those compounds present at higher levels in the wild type had terpene-like properties.
302 Notably, a terpene-encoding cluster (*sven_7101-7117*) was amongst a handful of metabolic clusters
303 whose expression decreased in the absence of Lsr2 (**Table 1; Table S1**). In contrast, the volatile
304 metabolites that were more abundant in the *lsr2* mutant appeared to be enriched for by-products of
305 specialized metabolic precursors (*e.g.* derivatives of pyruvate and acetyl-CoA).

306

307 **Modulating Lsr2 activity stimulates new metabolite production in diverse *Streptomyces* species**

308 The dramatic increase in metabolic production by the *lsr2* mutant in *S. venezuelae* prompted us
309 to test whether it was possible to exploit this activity and stimulate new metabolite production in other
310 streptomycetes. In *M. tuberculosis*, a dominant negative allele of *lsr2* has been reported, in which a
311 conserved Arg residue in the C-terminal DNA-binding domain is changed to an Ala residue (Gordon *et al.*,
312 2008). We constructed an equivalent *Streptomyces* variant (R82A mutant). Using EMSAs, we
313 confirmed that this protein was defective in its ability to bind DNA, and that it interfered with DNA
314 binding by the wild type protein (**Figure S10**). We also cloned this dominant negative allele behind a
315 highly active, constitutive (*ermE**) promoter on an integrating plasmid vector (**Figure 6A**), and
316 introduced this 'Lsr2 knockdown' construct into wild type *S. venezuelae* to test whether it was able to
317 phenocopy the *lsr2* mutant. Using a bioassay, we detected increased antibiotic production for this
318 strain, relative to one carrying an empty plasmid vector (**Figure S10**). We also introduced the construct

319 into the well-studied *S. coelicolor* strain, and observed copious production of the blue pigmented
320 metabolite actinorhodin when grown on a medium where this compound is not typically produced
321 (**Figure 6B**). Finally, we tested the construct in a small library of wild *Streptomyces* isolates. We
322 screened for new metabolite production using a bioassay to assess antibiotic production. We first
323 introduced the Lsr2 knockdown construct into strain WAC4718. This led to a significant increase in
324 growth inhibition of *M. luteus*, and new growth inhibition of *B. subtilis*, relative to the plasmid-alone
325 control strain (**Figure 6C**). We next introduced the knockdown and control constructs into four
326 additional wild isolates (**Figure 6D**), and tested their antibiotic production capabilities against the
327 indicator strain *M. luteus*. We observed new and/or increased antibiotic production for two strains
328 (WAC7072 and WAC7520), no change in growth inhibition for one strain (WAC5514), and reduced
329 activity in the final strain (WAC6377). Notably, these strains did not grow appreciably differently
330 compared with their empty plasmid-containing parent strain (e.g. **Figure S11**). These results suggested
331 our construct had the ability to downregulate Lsr2 activity in a wide range of streptomycetes, and could
332 serve as a broadly applicable means of stimulating antibiotic production in these bacteria.

333

334 **DISCUSSION**

335 The nucleoid-associated protein Lsr2 has been tied to virulence and environmental adaptation in
336 *Mycobacterium*, and like H-NS in *E. coli*, it has been proposed to function to repress the expression of
337 ‘foreign’ DNA (Gordon *et al.*, 2010; Gordon *et al.*, 2011). Here, we demonstrate a role for Lsr2 in
338 repressing the expression of laterally acquired sequences in *Streptomyces*, as well as in suppressing the
339 expression of antisense RNA, as has also been observed for H-NS. Uniquely in *Streptomyces*, however, it
340 appears that Lsr2 function has been co-opted for the control of specialized metabolism, and that the
341 cryptic/silent nature of many of these metabolic clusters is due to direct Lsr2 repression.

342

343 **Mechanism of Lsr2-mediated repression**

344 Previous work on Lsr2 from the mycobacteria has shown Lsr2 preferentially binds AT-rich DNA
345 (Gordon *et al.*, 2010; Gordon *et al.*, 2011), and our findings suggest that this is also the case in the
346 streptomycetes. Unlike more conventional transcription factors, we found that Lsr2 binding sites in *S.*
347 *venezuelae* tended to be quite broad, centring on AT-rich sequences, extending hundreds (or thousands)
348 of base-pairs, and frequently encompassing promoter regions (**Table S3**). In the proteobacteria, H-NS
349 can polymerize along the chromosome (Liu *et al.*, 2010; Lim *et al.*, 2012; Ryan Will *et al.*, 2018),
350 repressing transcription by shielding the DNA from binding by transcription factors or RNA polymerase.

351 It can also bridge disparate DNA segments (van der Valk *et al.*, 2017), repressing gene expression by
352 trapping RNA polymerase, and/or changing the local DNA architecture. Lsr2 repression in *S. venezuelae*
353 is consistent with both polymerization and bridging mechanisms. The larger binding sites, often
354 associated with transcriptional changes, could be the result of Lsr2 filamentation along the chromosome
355 in those regions. We also identified multiple specialized metabolic clusters having more than one Lsr2
356 binding site (see **Figure 3**). This was particularly notable within the right arm of the chromosome (**Table**
357 **1**). These sites were often smaller (**Table S3**), and it is possible that gene repression is achieved through
358 bridging between these sites.

359 Many of the Lsr2 binding sites identified here, however, were not associated with altered
360 transcription of their flanking genes. It is conceivable that these sites serve more of an architectural
361 role, with Lsr2 binding promoting chromosome organization and compaction. Binding at these sites may
362 also exert indirect effects on transcription, as a result of altered DNA structure and accessibility.

363 In this study, we focussed our attention on the DNA-binding activity of Lsr2, but it is worth
364 noting that post-transcriptional regulatory roles have been identified for related proteins. In particular,
365 H-NS can also bind RNA (Park *et al.*, 2010), where it stabilizes target transcripts and promotes their
366 translation. Notably, within the differentially expressed genes identified here, Lsr2 enhanced the
367 expression of 10% of these genes. These may be interesting candidates for future investigations aimed
368 at understanding alternative regulatory roles for Lsr2.

369

370 **Role for Lsr2 repression**

371 Our results suggest that Lsr2 functions both as a 'genome sentinel', and as a central governor of
372 specialized metabolism. It represses the expression of many genes that seem to have been recently
373 acquired based on conservation analysis. However, it also controls the expression of many well-
374 conserved clusters in *S. venezuelae*. It is not clear how *Streptomyces* species acquire their specialized
375 metabolic clusters. The clustered nature of specialized metabolic genes makes them amenable to
376 transfer between species through conjugation or transduction (*Streptomyces* are not naturally
377 competent for DNA transformation), although genomic studies have suggested that the transfer and
378 maintenance of entire clusters is relatively uncommon (McDonald and Currie, 2017). In many clusters,
379 the pathway-specific regulators (Williamson *et al.*, 2006; Fernández-Martínez *et al.*, 2014) and/or
380 resistance determinants (*e.g.* Flatt and Mahmud, 2007; Thaker *et al.*, 2013; Mak *et al.*, 2014) are
381 encoded near the ends of the cluster. Loss of either of these genetic elements during cluster transfer to

382 a recipient could lead to inappropriate cluster expression in the absence of a fail-safe mechanism
383 provided by proteins like Lsr2.

384 Within *S. venezuelae*, seven clusters lack an obvious pathway-specific regulator, and of these,
385 five are under Lsr2 control. Similarly, six of nine clusters lacking an associated transporter are affected
386 by Lsr2 (although resistance can be conferred by means other than transport, and not all specialized
387 metabolites function extracellularly). In the streptomycetes, Lsr2 may therefore act to protect the cell
388 from the toxic products of newly acquired clusters, until they are either integrated into existing
389 regulatory networks, or are lost from the cell. Widely conserved clusters controlled by Lsr2 (*e.g.*
390 siderophore/desferrioxamine and bacteriocin) likely represent instances of successful integration, where
391 Lsr2 control has evolved such that its repression can be alleviated under appropriate conditions.
392 However, not all specialized metabolic clusters are under Lsr2 control. The products of Lsr2-independent
393 clusters may be important for growth under laboratory conditions (and thus any Lsr2-mediated
394 repression may have been alleviated under our experimental conditions), or they may be largely benign
395 and/or have a low fitness cost associated with their production. On the other end of the spectrum are
396 the volatile compounds, many of which required Lsr2 for their production. It appears that the synthesis
397 of these molecules may be subject to different regulatory constraints than those of the specialized
398 metabolites.

399

400 **Control of Lsr2 expression and activity**

401 As Lsr2 governs the expression of the majority of specialized metabolic clusters in *S. venezuelae*,
402 it is critical to understand how its expression and activity are controlled. In the proteobacteria, factors
403 that impact H-NS expression and activity have been extensively studied; however, far less known about
404 what affects Lsr2 levels and function in the actinobacteria.

405 In the proteobacteria, *hns* expression is activated by multiple transcription factors (Falconi *et al.*,
406 1996; La Teana *et al.*, 2006), and is negatively regulated by both small RNAs and H-NS itself (Falconi *et al.*,
407 1993; Lalaouna *et al.*, 2015). In the actinobacteria, there is currently nothing known about the
408 transcriptional regulation of *lsr2*, although it likely governs its own expression: there is a large Lsr2
409 binding site that overlaps the *lsr2* promoter (Table S3), suggesting that, like H-NS, it negatively regulates
410 its own expression. How *lsr2* expression is activated, and whether it is also subject to post-
411 transcriptional regulation remains to be seen.

412 At a protein level, H-NS activity can be modulated by interaction with a multitude of proteins,
413 including association with paralogous proteins like StpA (Müller *et al.*, 2010). Intriguingly, all

414 streptomycetes encode a paralogous Lsr2-like protein, termed LsrL. Our data suggest that there exists
415 regulatory interplay between these proteins, with Lsr2 repressing *lsrL* expression. It will be interesting to
416 see whether LsrL associates with Lsr2 to form hetero-oligomers, and whether such an association alters
417 Lsr2 activity. Deleting *lsrL* did not have profound phenotypic consequences, at least under the
418 conditions we tested, so understanding its biological role in *Streptomyces* will require additional
419 investigation. Unlike the streptomycetes, the mycobacteria do not encode additional Lsr2-like proteins.
420 However, recent work in *M. tuberculosis* has suggested that Lsr2 can associate with the unrelated
421 nucleoid-associated protein HU (Datta *et al.*, 2019); whether an equivalent interaction occurs in
422 *Streptomyces* has yet to be determined. Lsr2 also appears to be subject to post-translational
423 modification, having been identified in several phospho-proteome screens conducted in *Streptomyces*
424 *coelicolor* (Parker *et al.*, 2010; Manteca *et al.*, 2011), although how phosphorylation affects Lsr2 activity
425 is currently unclear.

426 H-NS-mediated repression can be alleviated through competition for binding to similar
427 sequences by other transcription factors (Will *et al.*, 2015). Equivalent ‘counter-silencing’ mechanisms
428 have been reported for Lsr2 in the mycobacteria (Kurthkoti *et al.*, 2015). Given that at least a subset of
429 the Lsr2-controlled specialized metabolic clusters are expressed under particular growth conditions in *S.*
430 *venezuelae* (e.g. desferrioxamine, melanin), there must exist mechanisms to relieve Lsr2 repression in
431 the streptomycetes as well. Intriguing candidates for this could include global antibiotic regulators, or
432 cluster-situated regulators, and revealing how Lsr2 is integrated into the larger regulatory networks
433 governing specialized metabolism will be a major priority.

434

435 **Chromosome organization and the regulation of specialized metabolism**

436 Lsr2 is one of multiple nucleoid-associated proteins encoded by the streptomycetes, including
437 sIHF (Swiercz *et al.*, 2013), the HU proteins HupA and HupS (Salerno *et al.*, 2009), and BldC (Bush *et al.*,
438 2019). To date, only BldC binding and regulation has been thoroughly characterized, but unlike Lsr2, its
439 primary regulatory targets are developmental determinants, not specialized metabolic clusters.
440 Phenotypic analyses of *sIHF* and *hupS* mutants in *S. coelicolor* revealed major sporulation defects, in
441 contrast to the modest developmental delay observed for the *lsr2* mutant (Salerno *et al.*, 2009; Swiercz
442 *et al.*, 2013). Both mutations also impacted metabolism, with the *sIHF* mutant exhibiting both enhanced
443 and reduced production of pigmented antibiotics, depending on media conditions, and the *hupS* mutant
444 failing to produce the brown spore pigment in *S. coelicolor*. While a comprehensive analysis remains to

445 be conducted, neither sIHF nor HupS appear to function like Lsr2 in exerting global control over
446 specialized metabolism.

447 In the fungi, chromosome organization is governed by the histones which, like the nucleoid-
448 associated proteins in bacteria, function to both compact the chromosome and control gene expression.
449 Like *Streptomyces*, fungi possess a multitude of cryptic secondary metabolic clusters, and many of these
450 are silenced as a result of histone activity (Keller, 2018). Successful cluster activation has been achieved
451 by manipulating histone activity through altered acetylation or methylation (Pfannenstiel and Keller,
452 2019).

453 Given the broad conservation of Lsr2 across the streptomycetes, and its significant impact on
454 specialized metabolism in these bacteria, Lsr2 is an attractive candidate for activity modulation, like the
455 histones in fungi. Deleting *lsr2* may not be feasible in all *Streptomyces*, given recent studies suggesting
456 that it is an essential gene in some species (Najah *et al.*, 2019). However, our work here suggests that
457 downregulating Lsr2 activity may offer an effective approach to alleviating metabolic repression, and
458 can profoundly alter the metabolic output of a wide range of streptomycetes. Collectively, it may
459 provide a new avenue for accessing otherwise cryptic natural products in these metabolically gifted
460 bacteria, facilitating both our understanding of the chemical ecology associated with microbial signalling
461 and interactions, and our ability to identify new compounds for clinical development.

462

463 **MATERIALS AND METHODS**

464 **Bacterial strains, plasmids, oligonucleotides and culture conditions**

465 All strains and plasmids/cosmids are outlined in **Table S6**, while oligonucleotide information is
466 provided in **Table S7**. *S. venezuelae* strains were grown at 30°C on MS (soy flour-mannitol) agar, MYM
467 (maltose yeast extract mannitol) agar, YPD (yeast-peptone-dextrose) agar, and YP (yeast-peptone) agar,
468 or in liquid MYM medium prepared as described previously (Kieser *et al.*, 2000; Jones *et al.*, 2017). *S.*
469 *coelicolor* strains were grown on Difco nutrient agar plates, while wild *Streptomyces* isolates were grown
470 on ISP4 medium (Difco) supplemented with maltose (1 g/L), mannitol (1 g/L), sucrose (1 g/L) and
471 glycerol (1 g/L), or in Bennet's medium. *E. coli* strains were grown at 37°C on or in LB (Luria-Bertani)
472 medium or in liquid SOB (Super Optimal Broth) (Kieser *et al.*, 2000).

473

474 **Strain and plasmid construction**

475 An in-frame deletion of *lsr2* (*sven_3225*) was created using the ReDirect PCR targeting method
476 (Gust *et al.*, 2003). The *lsr2* coding region was replaced with the *aac(3)IV-oriT* resistance cassette, which

477 was subsequently excised using the yeast FLP recombinase to leave an 81 bp scar. The *aac(3)IV-oriT*
478 cassette was amplified from pIJ773 using the primer pair Sven3225disruptF and Sven3225disruptR2 to
479 generate an extended resistance cassette (oligonucleotide sequences listed in **Table S7**). Cosmid 1-C1
480 (<http://strepdb.streptomyces.org.uk/>) was introduced into *E. coli* BW25113 containing pIJ790, and the
481 *lsr2* coding region was replaced with the extended resistance cassette. Cosmid 1-C1 Δ *lsr2::aac(3)IV-oriT*
482 was confirmed both via PCR using the flanking primers sven3225F2 and sven3225R2, and through a
483 diagnostic restriction digest. The modified cosmid was then introduced into *S. venezuelae* by
484 conjugation. Two representative apramycin-resistant, kanamycin-sensitive null mutants were selected
485 for morphological analysis. Cosmid 1-C1 Δ *lsr2::aac(3)IV-oriT* was introduced into *E. coli* BT340 in which
486 the FLP recombinase was induced to excise the *aac(3)IV-oriT* cassette from the cosmid. The cosmid
487 backbone was then targeted to replace *bla* with the *hyg-oriT* cassette from pIJ10701 (Gust *et al.*, 2004).
488 The resulting cosmid was checked using PCR (**Table S7**) and restriction digest, prior to being mobilised
489 into *S. venezuelae* Δ *lsr2::aac(3)IV-oriT*. Hygromycin-resistant exconjugants were selected, and then
490 screened for a double cross-over event resulting in apramycin-sensitive, hygromycin-sensitive scarred
491 mutants that were confirmed by PCR (**Table S7**).

492 *S. venezuelae* Δ *lsr2* was complemented through cloning *lsr2*, together with 257 bp upstream and
493 293 bp downstream flanking sequences, into the *EcoRV*-digested integrative plasmid pIJ82. Gene
494 synthesis (GenScript) was used to generate a C-terminal triple FLAG-tagged variant
495 (DYKDHDGDYKDHDIDYKDDDDK, separated from the *Lsr2* sequence by a triple glycine linker) bearing the
496 same upstream and downstream sequences as the native complementation construct. This synthesized
497 sequence was flanked by *Bgl*III sites, which facilitated subcloning into the *Bam*HI site of the integrative
498 plasmid pIJ10706 (pIJ82 and pIJ10706 are identical except that pIJ10706 uses the *aac(3)IV* promoter to
499 drive expression of *hyg*). Both *lsr2*-carrying plasmids were introduced individually into the *lsr2* mutant
500 and assessed for their ability to complement the developmental delay observed on solid MYM.

501 An in-frame deletion of *lsrL* (*sven_3832*) was created using the ReDirect PCR targeting method
502 (Gust *et al.*, 2003) described above. The *lsrL* coding region was replaced with the *aac(3)IV-oriT* resistance
503 cassette in cosmid 4E19 and conjugated from the non-methylating *E. coli* strain ET12567 (MacNeil *et al.*,
504 1992) containing pUZ8002 (Paget *et al.*, 1999) into *S. venezuelae*. Two representative apramycin-
505 resistant, kanamycin-sensitive null mutants were confirmed by PCR (**Table S7**) and were subjected to
506 morphological and metabolic analyses.

507 To mutate *sven_6229*, CRISPR-Cas-mediated mutagenesis was used (Cobb *et al.*, 2015), with
508 minor alterations to the published protocol. Briefly, a 32 nucleotide deletion, along with an in-frame

509 stop codon, was introduced into *sven_6229*. The guide RNA sequence was cloned into the *Bsbl* site of
510 pCRISPomyces2, following the annealing of the overlapping oligonucleotides Sven6229 GuideF and
511 Sven6229 GuideR (**Table S7**). The editing template was generated by first amplifying fragments
512 upstream (Sven6229 UpF/R) and downstream (Sven6229 DownF/R) of the guide RNA sequences. These
513 sequences were then joined by overlap extension PCR, before being digested and cloned into the *XbaI*
514 site of the guide RNA-carrying pCRISPomyces vector. Sequence integrity of both the guide RNA and
515 editing template was confirmed by sequencing. The resulting plasmid was conjugated into the *lsr2*
516 mutant (**Table S6**), and exconjugants were selected for using apramycin and nalidixic acid. Colonies were
517 then streaked on MS agar plates without antibiotic supplementation, and were screened for the desired
518 deletion using the Sven6229 GuideF and Sven6229 DownR primers. Candidate deletion mutants were
519 subjected to a final PCR check, using Sven6229 UpR and Sven6229 ConR, and the resulting product was
520 sequenced to confirm the mutation.

521 To investigate the effects of AT-content on Lsr2 binding and gene expression, we focussed on a
522 validated Lsr2 binding site between *sven_5106* and *sven_5107*, where the expression of these genes was
523 increased upon loss of Lsr2, suggesting Lsr2 repression. To clone a ~9 kb DNA fragment spanning
524 *sven_5105-5107*, the TOPO® TA cloning kit was used as per the manufacture's instructions. Briefly, the
525 fragment was amplified using the Phusion proofreading polymerase (New England Biolabs) with
526 oligonucleotides Sven5105_5107F and Sven5105_5107R (**Table S7**), a 72°C annealing temperature, and
527 cosmid Sv-3-D04 (**Table S6**) as template. The amplified product was purified by gel extraction, and was
528 then incubated with *Taq* polymerase and dATP at 72°C for 15 min. Four microlitres of the resulting A-
529 tailed product were mixed with salt solution and pCR®2.1-TOPO® vector provided in the cloning kit,
530 before being introduced into Subcloning Efficiency™ DH5α™ competent cells (ThermoFisher
531 Scientific). The *sven_5105-5107* containing plasmid was verified using restriction enzyme digestion and
532 sequencing. To create mutant variants, synthetic gene fragments were generated and amplified using
533 oligonucleotides Sven5106_5107F and Sven5106_5107R (**Table S7**). The amplified products were cloned
534 between unique *NheI* and *AvrII* sites within the *sven5105-07* sequences. The designed mutations were
535 confirmed by restriction digestion and sequencing. All validated *sven_5105-5107* variants (wild type
536 and mutants) were excised from the TOPO vector using *XbaI* and *SpeI*, and cloned into the *SpeI* site of
537 pRT801. Constructs were then conjugated into wild type *S. venezuelae* and Δ *lsr2* mutant strains (for
538 expression analysis), and the Δ *lsr2* mutant strains complemented with either *lsr2* or *lsr2-3xFLAG* (for
539 CHIP analyses).

540

541 ***Streptomyces* cell extract preparation, SDS-PAGE, and immunoblotting**

542 Cell extracts were prepared from a 1 mL aliquot of *S. venezuelae* cells grown in liquid MYM
543 medium. The protein extracts were separated using 15% SDS-PAGE and were stained with Coomassie
544 brilliant blue R-250. Equivalent amounts of total protein were loaded onto a second 15% SDS-PAGE, and
545 following transfer to PVDF membranes, were subjected to immunoblotting with anti-FLAG antibody
546 (1:1,500; Sigma) and anti-rabbit IgG horseradish peroxidase (HRP)-conjugated secondary antibodies
547 (1:3,000; Cell Signaling).

548

549 **Lsr2 overexpression, purification and electrophoretic mobility shift assays (EMSAs)**

550 *lsr2* amplified using primers NdeISven3225F and BamHISven3225R (**Table S7**) was digested and
551 the product cloned into similarly digested pET15b (**Table S7**). After sequencing, this construct was
552 introduced into *E. coli* Rosetta cells (**Table S7**). Overexpression of 6×His-*lsr2* was achieved by growing
553 cultures at 37°C to an OD₆₀₀ of 0.5, and then adding 0.5 mM IPTG (isopropyl β-D-1-
554 thiogalactopyranoside). Cells were grown for a further 3 h at 30°C before harvesting and resuspending in
555 binding buffer (50 mM NaH₂PO₄, 300 mM NaCl and 10 mM imidazole, pH 8.0) containing 1 mg/mL
556 lysozyme and one complete mini EDTA-free protease inhibitor pellet (Roche). Cell suspensions were
557 incubated on ice for 20 min before sonication. 6×His-Lsr2 was purified by binding to 1 mL Ni-NTA
558 agarose (Invitrogen), after which the resin was collected and the bound protein was washed with
559 binding buffer supplemented with increasing concentrations of imidazole. Purified proteins were
560 ultimately eluted using 500 mM imidazole. Purified protein was exchanged into storage buffer (20 mM
561 Tris-HCl, pH 8, 150 mM NaCl, 25% glycerol and 1.4 mM β-mercaptoethanol) using an Amicon Ultra-15
562 Centrifugal Filter with a 3 kDa cut-off. Bradford assays were conducted to measure protein
563 concentrations.

564 EMSAs were performed using 124 – 280 bp probes amplified by PCR and 5'-end-labelled with [γ-
565 ³²P]dATP (primers prefixed “emsa” are listed in **Table S7**). Increasing concentrations of Lsr2 (0–5 μM)
566 were combined with either 1 or 10 nM probe, 1 mg/mL bovine serum albumin (BSA) and binding buffer
567 (10 mM Tris, pH 7.8, 5 mM MgCl₂, 60 mM KCl and 10% glycerol). Each reaction was incubated for 10 min
568 at room temperature, followed by 30 min on ice prior to adding a glycerol-based loading dye and
569 running on a 12% native polyacrylamide gel. To test binding specificity, competition assays were
570 established in which increasing concentrations (0-160 nM) of unlabeled probe were added together with
571 4 nM labelled probe and 1 μM Lsr2, to the EMSA reactions described above. Gels were exposed to a
572 phosphor plate for 1 h, before being visualized using a phosphorimager (Typhoon FLA 9500).

573

574 **RNA isolation and RT-(q)PCR**

575 Wild type *S. venezuelae* and the Δ *lsr2* mutant strain were grown in 300 mL MYM cultures in
576 duplicate. After 8 h (vegetative growth), 12 h (early mycelial fragmentation) and 18 hours (late mycelial
577 fragmentation/ sporulation), density at OD₄₅₀ was measured, and a 60-90 mL sample was harvested.
578 Subsequent experiments involved growing wild type and Δ *lsr2* mutant strains carrying *sven_5105-*
579 *sven_5107* variants on an integrating plasmid. These strains were grown in duplicate, in 50 mL MYM
580 liquid medium for 18 h. In all cases, RNA was isolated as described in Moody *et al.* (Moody *et al.*, 2013),
581 using a modified guanidium thiocyanate protocol (Chomczynski and Sacchi, 1987). Primers HrdBF and
582 HrdBR, or SVEN4987F/SVEN4987R (**Table S7**) were used for PCR checks, alongside a quantified
583 chromosomal DNA control, to confirm any DNA contamination was <0.005%.

584 Reverse transcription (RT) reactions were performed as described previously (Haiser *et al.*, 2009;
585 Moody *et al.*, 2013). In brief, gene-specific reverse primers (**Table S7**), or random oligonucleotides were
586 annealed to 1 µg of total RNA prior to cDNA synthesis using SuperScript® III reverse transcriptase
587 (Invitrogen) (wild type and mutant) or Lunascript™ RT (New England Biolabs) (*sven5105-5107* variants),
588 respectively.

589 To validating RNA-sequencing results, two microlitres of the resulting cDNA were used as
590 template DNA for PCR, with a 58°C annealing temperature. The number of cycles was optimized to
591 ensure that amplification was occurring within the linear range of the reaction (33 cycles for *sven_0514*,
592 *sven_6216*, *sven_6264* and *hrdB* and 30 cycles for *sven_0493* and *sven_5135*). Negative control
593 reactions were run to confirm the absence of genomic DNA contamination in the RNA samples, and
594 involved adding an equivalent volume of a reverse transcription reaction in which nuclease free water
595 had been added in place of reverse transcriptase. All reverse transcription reactions and PCR
596 amplifications were carried out in duplicate, using RNA isolated from two independent cultures.

597 For the *sven_5105-5107* variant-containing strains, 2.5 µL of cDNA (1:4) were used as template
598 for qPCR. Primers 5106F/5106R were used to amplify target gene from cDNA with a 55°C annealing
599 temperature. 'No RT' samples were run to confirm no DNA contamination. All samples were assessed in
600 biological duplicate and technical triplicate. qPCR data were normalized to *rpoB* and were analyzed using
601 a relative quantification method (2^{-DDC_T}) (Livak and Schmittgen, 2001).

602

603 **RNA-seq sample preparation and data analysis**

604 Library construction and sequencing were performed by the Farncombe Metagenomics Facility,

605 McMaster University, Hamilton, Canada. Total RNA (1.7 μ g) from each sample was subjected to rRNA
606 depletion using RiboZero (Epicentre), as per the manufacturer's instructions. Library preparation was
607 performed using the NEBNext Ultra Directional RNA Library Prep Kit (NEB), including double-AMPure
608 bead (Beckman Coulter) size selection. Following quality control, libraries were pooled in equimolar
609 amounts and sequenced over two lanes of the HiSeq 1500 using the TruSeq Rapid (v1) chemistry with
610 onboard cluster generation and a 1 \times 75 bp protocol.

611 Raw sequencing reads were trimmed to remove low-quality 3' ends using PrinSeq (Schmieder
612 and Edwards, 2011). Trimmed reads were checked for quality using FastQC
613 (www.bioinformatics.babraham.ac.uk/projects/fastqc/) and aligned to the *S. venezuelae* ATCC 10712
614 genome sequence using Bowtie2 (Langmead *et al.*, 2009).

615 The resultant SAM files were converted to BAM format, sorted by genomic position and indexed
616 to create bai files (Li *et al.*, 2009). The BAM files were analyzed both visually using Integrated Genomics
617 Viewer (Version 2.3.60) (Robinson *et al.*, 2011), and using Rockhopper2 (Tjaden, 2015). We assigned a
618 cut-off for significance using a *p*-value adjusted for multiple testing that was less than 0.01 (*q*-value), and
619 filtered for genes displaying a fold change greater than four.

620

621 **Chromatin immunoprecipitation**

622 *S. venezuelae* Δ *lsr2* was complemented using an integrating plasmid (pIJ10706/pIJ82) carrying
623 either wild type *lsr2* or *lsr2-3 \times FLAG* (Table S6). Each culture was then grown in 300 mL MYM cultures in
624 duplicate. After 18 h, the density at OD₄₅₀ was measured and the developmental progression of each
625 strain was monitored by light microscopy. A 1 mL sample was then taken for immunoblot analysis, and
626 an 80 mL sample was transferred to a sterile flask. Formaldehyde was added to a final concentration of
627 1% (vol/vol) to cross-link protein to DNA, after which cultures were incubated for a further 30 min.
628 Glycine was then added to a final concentration of 125 mM. Immunoprecipitation was carried out as
629 described in Bush *et al.* (Bush *et al.*, 2013), using Anti-FLAG (DYKDDDDK) affinity gel (BioTools).
630 Immunoprecipitation, and subsequent sequencing, were done in duplicate.

631 Library construction and sequencing were performed by the Farncombe Metagenomics Facility,
632 McMaster University, Hamilton, Canada. The NEBNext Ultra DNA Library Prep Kit was used for library
633 preparation, starting with 10 ng of the sheared ChIP DNA and including a double-AMPure bead
634 (Beckman Coulter) size selection. Following quality control, libraries were pooled in equimolar amounts
635 and sequenced on one MiSeq run using a 2 \times 75 bp (v3) configuration.

636

637 **ChIP-seq data analysis**

638 The reads in the fastq files were first checked for quality using FastQC
639 (www.bioinformatics.babraham.ac.uk/projects/fastqc/), then aligned to the *S. venezuelae* ATCC 10712
640 genome (GenBank accession number NC_018750) using Bowtie2 (Langmead *et al.*, 2009). The resultant
641 SAM files were converted to BAM format, sorted by genomic position and indexed to create BAI files (Li
642 *et al.*, 2009). The BAM files were visualized using Integrated Genomics Viewer (Version 2.3.60)
643 (Robinson *et al.*, 2011), and were subjected to quantitative analysis.

644 *MACS2* was run from the command line to normalize all *Isr2* and the *Isr2-3xFLAG* samples
645 against total DNA with the mappable genome size set at 7.92×10^6 (90% of the *S. venezuelae* genome) to
646 generate BED files (Zhang *et al.*, 2008). The BED files were in turn used to generate a CSV sample sheet
647 that was read into the R package for statistical computing (Team, 2013) using the *read* function of the
648 *DiffBind* package (Stark and Brown, 2011). The *dba.count* function of the *DiffBind* package was used to
649 calculate a binding matrix with scores based on read counts for each sample. The *dba.contrast* function
650 of the *DiffBind* package was then used to compare the *Isr2* (negative control) samples with the *Isr2-*
651 *3xFLAG* samples. The *dba.analyze* function of the *DiffBind* package was used to run an *edgeR* analysis
652 that identified sites that were significantly differentially bound [having a *p*-value adjusted for multiple
653 testing that was less than 0.01 (*q*-value)]. These differentially bound sites were retrieved using the
654 *dba.report* function.

655

656 **ChIP-quantitative PCR**

657 Strains were grown in 10 mL of MYM medium overnight, before being subcultured in duplicate
658 into 50 mL of MYM medium. After incubating for 18 h, formaldehyde was added to a final concentration
659 of 1% (v/v) to cross-link protein to DNA. The cultures were incubated for an additional 30 min, at which
660 time glycine was added to a final concentration of 125 mM. Immunoprecipitation was performed as
661 described above, only using the FLAG M2 antibody (Sigma).

662 To quantify the abundance of target genes of interest in the ChIP DNA, 20 μ L qPCR reactions
663 were prepared using Luna[®] Universal qPCR Master Mix (New England Biolabs) and 2.5 μ L of ChIP DNA
664 (1:10) as template. Primers 0926F/0926R and 5105F/5105R (**Table S7**) were used to amplify target gene
665 from ChIP DNA with a 55°C annealing temperature. qPCR data was then analyzed using DART-PCR
666 (Peirson *et al.*, 2003).

667

668 **Phylogenetic analysis of *Streptomyces* species**

669 Phylogenetic analysis was conducted based on the concatenated protein sequences encoded by
670 selected single-copy phylogenetic marker genes *serS*, *rpoB*, *secY*, and *rplB*. These sequences were
671 extracted from the complete genome sequences of the different streptomycetes, as well as from an
672 outgroup (*Bacillus subtilis*), all of which were accessed using the NCBI database. Alignments were
673 generated using ClustalX2 (Larkin *et al.*, 2007) using a neighbor joining cluster algorithm, with iteration
674 at each alignment step and 1000 bootstrap replications. The phylogenetic tree was visualised using
675 FigTree v1.4 (<http://tree.bio.ed.ac.uk/software/figtree>).

676

677 **Specialized metabolite extraction and analysis**

678 *S. venezuelae* WT and Δ *lsr2* strains were grown in triplicate as a lawn on MYM agar over a
679 timecourse of 3, 5 and 7 days. The entirety of each plate (as well as an MYM agar control) was
680 macerated in 25 mL *n*-butanol, sonicated for 5 min in a Branson 2520 tabletop ultrasonic cleaner and
681 shaken overnight at 4°C. The agar was removed by passing through a milk filter, then Whatman filter
682 paper, after which the solvent was split into two aliquots and dried down in a GeneVac. The residue was
683 reconstituted in either 500 μ L 50% methanol for bioassays, or 1 mL of 1:1 MeCN:H₂O for LC-MS analysis.

684 LC-MS analysis was performed on a Waters Alliance Acquity UPLC system coupled to a Xevo
685 G2S-QToF. A 10 μ L aliquot was taken and diluted with 90 μ L 1:1 MeCN:H₂O, and 10 μ L of this diluted
686 solution were injected onto a Phenomenex Kinetex Biphenyl column (1.7 μ m , 2.1 x 100 mm).

687 The samples were separated using a gradient of 5% to 95% acetonitrile (0.1% [vol/vol] formic
688 acid) at 40°C over 25 min, with a flow rate of 0.4 mL/min. Positive electrospray ionization was
689 performed and the ions were scanned over a mass range of 100 to 1200 Da. Data were analyzed using
690 MZmine 2 software (Pluskal *et al.*, 2010).

691 For soluble metabolites, and quantitation of the known metabolites shown in Figure 4C, cultures
692 grown in MYM liquid medium for 3, 4, or 5 days were centrifuged, and the supernatant lyophilized. The
693 lyophile was redissolved in 10 mL of 50:50 acetonitrile/water and shaken on a rotary shaker for 1 h.
694 After centrifugation to remove particulates, samples were analyzed on an Agilent UPLC-QTOF. Injections
695 of 2 μ L were separated on Zorbax Eclipse plus C18 column (2.1 mm x 50 mm) and a gradient of 0-1 min
696 isocratic 100%A, 1-17 min gradient from 100-0% A, and 17-20 min isocratic 100% B, where A is 98%
697 water, 2% methanol, 0.1% formic acid and B is 100% methanol, 0.1% formic acid, at a flow rate of 0.4
698 mL/min. Samples were measured in positive and negative ionization modes to gain the greatest
699 coverage. Samples were analyzed in technical triplicates and key features were assessed in biological
700 duplicates. Fragmentation analysis of features of interest was performed with a collision energy of 25 V.

701 Antibiotic bioassays were performed by testing methanol extracts of *S. venezuelae* grown for 1
702 to 3 days against *Micrococcus luteus*. Twenty microliters of each extract was applied to a Whatman
703 antibiotic assay disc and applied to a lawn of LB inoculated with a 25-fold dilution of the *M. luteus*
704 indicator strain grown to mid-exponential phase. The plates were incubated overnight at 30°C before
705 measuring the size of the zone of clearing. Bioassays for wild *Streptomyces* were performed by growing
706 isolates (knockdown- and plasmid-control containing) on ISP4 supplemented medium for 6 days at 30°C.
707 Overnight cultures of indicator strains (*M. luteus* or *B. subtilis*) were mixed 1% soft nutrient agar, which
708 was allowed to solidify before being overlaid atop the wild *Streptomyces* strains, after which the
709 cultures were incubated overnight at 37°C.

710

711 **Synthesis of N-acetyl-chloro-tryptophan standards**

712 Synthesis of *N*-acetyl-5-chloro-L-tryptophan was achieved using Wang resin (50 mg, 1 mmol/g
713 loading), which was swollen in anhydrous dimethylformamide (DMF). Fmoc-5-chloro-L-Trp-OH (57.5 mg,
714 0.125 mmol, 2.5 eq.) was dissolved in 5 mL 9:1 DMF:dichloromethane (DCM) and cooled to 0°C.
715 Diisopropylcarbodiimide (DIC) (6.3 mg, 0.050 mmol, 1 eq.) was added in minimal DCM. The reaction was
716 stirred for 30 min at 0°C, in a flask fitted with a drying tube. The anhydride mixture was added to the
717 swollen resin, after which DMAP (0.6 mg, 5 µmol, 0.1 eq.) was added, and the flask was then periodically
718 agitated at room temperature for 2 h. The resin was washed in 3 × 10 mL DMF, followed by 3 × 10 mL
719 DCM. The Fmoc group was removed by the addition of 10 mL 20% (V/V) piperidine in DMF, after which
720 the suspension was agitated for 20 min. The resin was washed as above, before acetylation was carried
721 out with the addition of acetic anhydride (5.0 µL, 0.05 mmol, 1 eq.) and diisopropylethylamine (DIPEA)
722 (1 µL, 5 µmol, 0.1 eq.) in 5 mL DMF. The resulting suspension was agitated for 30 min at room
723 temperature. The resin was washed as above, prior to cleavage being carried out with 10 mL 95% TFA,
724 2.5% triethylsilane, 2.5% DCM for 30 min. The eluent was then collected and evaporated to dryness.
725 Analysis by LC-MS was completed without any further purification.

726 To synthesize *N*-acetyl-7-chloro-L-tryptophan, 7-chloro-L-Trp-OH (24 mg, 0.1 mmol) was
727 dissolved in 20 µL 50 mM ammonium bicarbonate. Fifty microliters of an acetylation mixture (20 µL
728 acetic anhydride, 60 µL methanol) were added to the amino acid, after which the mixture was agitated
729 for 1 h at room temperature. The solvent was evaporated to dryness and the resulting product was
730 analyzed without additional purification.

731

732 **Analysis of volatile metabolites**

733 Volatile metabolites in the headspace of culture supernatants were concentrated, analyzed, and
734 relatively quantified using headspace solid-phase microextraction coupled to two-dimensional gas
735 chromatography time-of-flight mass spectrometry (HS-SPME-GC×GC-TOFMS), as described previously
736 (Jones *et al.*, 2017). Four millilitres of culture supernatants were transferred to 20 mL air-tight
737 headspace vials and sealed with a PTFE/silicone cap (Sigma-Aldrich). A 2 cm triphasic solid-phase
738 microextraction (SPME) fiber consisting of polydimethylsiloxane, divinylbenzene, and carboxen (Supelco)
739 was suspended in the headspace of the supernatant for 30 min at 37°C with 250 rpm shaking.

740 The SPME fiber was injected into the inlet of a Pegasus 4D (LECO Corp.) GC×GC-TOFMS
741 equipped with a rail autosampler (Gerstel), and fitted with a two-dimensional column set consisting of
742 an Rxi-624Sil [60 m × 250 μm × 1.4 μm (length × internal diameter × film thickness)] first column and
743 Stabilwax (Crossbond Carbowax polyethylene glycol; 1 m × 250 μm × 0.5 μm) second column (Restek). A
744 splitless injection was performed, with the front inlet set to 270°C. The main oven containing column 1
745 was held at 35°C for 30 s, and then ramped at 3.5°C/min to a final temperature of 230°C. The secondary
746 oven containing column 2 and cryogenic modulator were heated in-step with the main over with +5°C
747 and +30°C offsets, respectively. The modulation period was set at 2.0 s, with hot- and cold-pulses
748 alternating every 0.5 s. The transfer line temperature was set at 250°C. Mass spectra were collected
749 over a range of 30-500 *m/z*, with an acquisition rate of 200 spectra/s, an ion source temperature of
750 200°C, and a detector voltage offset of +50 V.

751 Alignment of peaks across chromatograms was performed using the Statistical Compare feature
752 of ChromaTOF (LECO Corp.). An inter-chromatogram mass spectral match score ≥ 600 (out of 1000) and
753 maximum first and second dimension retention time deviations of 6 s and 0.15 s, respectively, were
754 required for peak alignment. Only peaks detected at a signal-to-noise ratio of ≥ 50:1 in one or more
755 chromatogram were considered for subsequent analyses. Mass spectra were compared with the
756 National Institute of Standards and Technology (NIST) 2011 mass spectral library, and a forward match
757 score ≥ 700 (out of 1000) was required for putative compound identification. When possible, putative
758 identifications were affirmed by comparing experimentally-determined linear retention indices (using C₆
759 to C₁₅ straight-chain alkanes, Sigma-Aldrich) with previously-reported values for both polar and non-
760 polar column configurations.

761 Relative compound abundances (measured in total ion chromatogram (TIC)) were log₁₀-
762 transformed, mean-centered, and unit scaled prior to statistical analysis. The non-parametric Mann-
763 Whitney U-test (Mann and Whitney, 1947) with Benjamini-Hochberg correction (Benjamini and

764 Hochberg, 1995) was used to identify volatile metabolites that were significantly different in relative
765 compound abundance ($p < 0.05$ after correction) between WT and Δ *lsr2* strains.

766

767 **Construction of Lsr2 knockdown construct**

768 We created the dominant negative R82A point mutant variant of Lsr2 using overlap extension PCR.
769 Briefly, two products were generated using primers sven3225F/R82Asven3225R and
770 R82Asven3225F/sven3225R (**Table S7**). The resulting products were gel purified, before being mixed
771 together in a 1:1 molar ratio for subsequent stitching together and amplification. Amplification was
772 achieved using phosphorylated oligonucleotides sven3225F and sven3225R. The resulting product was
773 purified and cloned into pIJ82, and construct integrity was confirmed by sequencing. The R82A mutant
774 variant was then re-amplified using NdeI3225F and PacI3225R (to remove its native promoter, which is
775 subject to negative autoregulation), digested with *NdeI* and *PacI*, and cloned into the same restriction
776 enzyme sites in pIJ12551, downstream of the constitutive, highly active *ermE** promoter (**Tables S8** and
777 **S9**). Construct integrity was confirmed by sequencing before being introduced by conjugation into *S.*
778 *venezuelae*, *S. coelicolor*, and five different wild *Streptomyces* isolates from the Wright actinomycete
779 collection (WAC4718, WAC5514, WAC6377, WAC7072, and WAC7520).

780

781

782 **ACKNOWLEDGEMENTS**

783 We wish to thank Michael Hewak, Talha Qureshi, Dan Seale, Lilian Raphael, and Christine Pham for
784 technical assistance, Stephen Miller for his computational/data mining expertise, and Gerry Wright for
785 access to his library of wild *Streptomyces* species. We are also grateful to Mervyn Bibb and Govind
786 Chandra (John Innes Centre), Ben Evans (McMaster University), and Will Navarre and Jun Liu (University
787 of Toronto) for helpful discussions. This work was supported by Cystic Fibrosis Canada (to JN and MAE),
788 the Canadian Institutes of Health Research (to MAE) and the Boris Family Foundation (to MAE). E.J.G. was
789 supported by a Department of Foreign Affairs and International Trade fellowship, and the Drug Safety
790 and Efficacy Cross-disciplinary Training program from the Canadian Institutes of Health Research.

791

792

793 **REFERENCES**

794 Bailey, T.L., Boden, M., Buske, F.A., Frith, M., Grant, C.E., Clementi, L., *et al.* (2009) MEME Suite: Tools
795 for motif discovery and searching. *Nucleic Acids Res* **37**.

796

797 Barka, E.A., Vatsa, P., Sanchez, L., Gaveau-Vaillant, N., Jacquard, C., Klenk, H.-P., *et al.* (2016) Taxonomy,

798 physiology, and natural products of actinobacteria. *Microbiol Mol Biol Rev* **80**: 1–43.
799
800 Benjamini, Y., and Hochberg, Y. (1995) Controlling the false discovery rate: a practical and powerful
801 approach to multiple testing. *J R Stat Soc Ser B* **57**: 289–300.
802
803 Bentley, S., Chater, K., Cerdeño-Tárraga, A.-M., Challis, G.L., Thomson, N.R., James, K.D., *et al.* (2002)
804 Complete genome sequence of the model actinomycete *Streptomyces coelicolor* A3(2). *Nature* **417**:
805 141–147.
806
807 Bush, M.J., Bibb, M.J., Chandra, G., Findlay, K.C., and Buttner, M.J. (2013) Genes required for aerial
808 growth, cell division, and chromosome segregation are targets of *whiA* before sporulation in
809 *Streptomyces venezuelae*. *mBio* **4**: e00684-13.
810
811 Bush, M.J., Chandra, B., Al-Bassam, M.M., Findlay, K.C., and Buttner, M.J. (2019) BldC delays entry into
812 development to produce a sustained period of vegetative growth in *Streptomyces venezuelae*. *mBio* **10**:
813 pii: e02812-18.
814
815 Castang, S., McManus, H.R., Turner, K.H., and Dove, S.L. (2008) H-NS family members function
816 coordinately in an opportunistic pathogen. *Proc Natl Acad Sci* **105**: 18947–18952.
817
818 Chandra, G., and Chater, K.F. (2014) Developmental biology of *Streptomyces* from the perspective of 100
819 actinobacterial genome sequences. *FEMS Microbiol Rev* **38**: 345–379.
820
821 Chomczynski, P., and Sacchi, N. (1987) Single-step method of RNA isolation by acid guanidinium
822 thiocyanate-phenol-chloroform extraction. *Anal Biochem* **162**: 156–159.
823
824 Cobb, R.E., Wang, Y., and Zhao, H. (2015) High-efficiency multiplex genome editing of *Streptomyces*
825 species using an engineered CRISPR-Cas system. *ACS Synth Biol* **4**: 723–728.
826
827 Craney, A., Ahmed, S., and Nodwell, J. (2013) Towards a new science of secondary metabolism. *J*
828 *Antibiot (Tokyo)* **66**: 387–400.
829
830 Dame, R.T., Noom, M.C., and Wuite, G.J.L. (2006) Bacterial chromatin organization by H-NS protein
831 unravelled using dual DNA manipulation. *Nature* **444**: 387–390.
832
833 Dame, R.T., Wyman, C., and Goosen, N. (2000) H-NS mediated compaction of DNA visualised by atomic
834 force microscopy. *Nucleic Acids Res* **28**: 3504–3510.
835
836 Daniel-Ivad, M., Hameed, N., Tan, S., Dhanjal, R., Socko, D., Pak, P., *et al.* (2017) An engineered allele of
837 *afsQ1* facilitates the discovery and investigation of cryptic natural products. *ACS Chem Biol* **12**: 628–634.
838
839 Datta, C., Jha, R.K., Ahmed, W., Ganguly, S., Ghosh, S., and Nagaraja, V. (2019) Physical and functional
840 interaction between nucleoid-associated proteins HU and Lsr2 of *Mycobacterium tuberculosis* : altered
841 DNA binding and gene regulation. *Mol Microbiol* doi: 10.1111/mmi.14202.
842
843 Dong, C., Flecks, S., Unversucht, S., Haupt, C., Pée, K.-H. van, and Naismith, J.H. (2005) Tryptophan 7-
844 halogenase (PrnA) structure suggests a mechanism for regioselective chlorination. *Science* **309**: 2216–
845 2219.

- 846
847 Dorman, C.J. (2007) H-NS, the genome sentinel. *Nat Rev Microbiol* **5**: 157–161.
848
- 849 Dorman, C.J. (2014) H-NS-like nucleoid-associated proteins, mobile genetic elements and horizontal
850 gene transfer in bacteria. *Plasmid* **75**: 1–11.
851
- 852 Falconi, M., Brandi, A., La Teana, A., Gualerzi, C.O., and Pon, C.L. (1996) Antagonistic involvement of FIS
853 and H-NS proteins in the transcriptional control of *hns* expression. *Mol Microbiol* **19**: 965–975.
854
- 855 Falconi, M., Higgins, N.P., Spurio, R., Pon, C.L., and Gualerzi, C.O. (1993) Expression of the gene encoding
856 the major bacterial nucleoid protein H-NS is subject to transcriptional auto-repression. *Mol Microbiol* **10**:
857 273–282.
858
- 859 Fernández-Martínez, L.T., Borsetto, C., Gomez-Escribano, J.P., Bibb, M.J., Al-Bassam, M.M., Chandra, G.,
860 and Bibb, M.J. (2014) New insights into chloramphenicol biosynthesis in *Streptomyces venezuelae* ATCC
861 10712. *Antimicrob Agents Chemother* **58**: 7441–7450.
862
- 863 Flärdh, K., and Buttner, M.J. (2009) *Streptomyces* morphogenetics: dissecting differentiation in a
864 filamentous bacterium. *Nat Rev Microbiol* **7**: 36–49.
865
- 866 Flatt, P.M., and Mahmud, T. (2007) Biosynthesis of aminocyclitol-aminoglycoside antibiotics and related
867 compounds. *Nat Prod Rep* **24**: 358–392.
868
- 869 Gao, C., Hindra, Mulder, D., Yin, C., and Elliot, M.A. (2012) Crp is a global regulator of antibiotic
870 production in *Streptomyces*. *mBio* **3**: pii: e00407-12.
871
- 872 Gordon, B.R.G., Imperial, R., Wang, L., Navarre, W.W., and Liu, J. (2008) Lsr2 of *Mycobacterium*
873 represents a novel class of H-NS-like proteins. *J Bacteriol* **190**: 7052–7059.
874
- 875 Gordon, B.R.G., Li, Y., Cote, A., Weirauch, M.T., Ding, P., Hughes, T.R., *et al.* (2011) Structural basis for
876 recognition of AT-rich DNA by unrelated xenogeneic silencing proteins. *Proc Natl Acad Sci* **108**: 10690–
877 10695.
878
- 879 Gordon, B.R.G., Li, Y., Wang, L., Sintsova, A., Bakel, H. van, Tian, S., *et al.* (2010) Lsr2 is a nucleoid-
880 associated protein that targets AT-rich sequences and virulence genes in *Mycobacterium tuberculosis*.
881 *Proc Natl Acad Sci* **107**: 5154–5159.
882
- 883 Gust, B., Challis, G.L., Fowler, K., Kieser, T., and Chater, K.F. (2003) PCR-targeted *Streptomyces* gene
884 replacement identifies a protein domain needed for biosynthesis of the sesquiterpene soil odor
885 geosmin. *Proc Natl Acad Sci U S A* **100**: 1541–1546.
886
- 887 Gust, B., Chandra, G., Jakimowicz, D., Yuqing, T., Bruton, C.J., and Chater, K.F. (2004) λ Red-mediated
888 genetic manipulation of antibiotic-producing *Streptomyces*. *Adv Appl Microbiol* **54**: 107–128.
889
- 890 Haiser, H.J., Yousef, M.R., and Elliot, M.A. (2009) Cell wall hydrolases affect germination, vegetative
891 growth, and sporulation in *Streptomyces coelicolor*. *J Bacteriol* **191**: 6501–6512.
892
- 893 Hopwood, D.A. (2007) *Streptomyces in Nature and Medicine: The Antibiotic Makers*. Oxford University

- 894 Press.
895
896 Inahashi, Y., Zhou, S., Bibb, M.J., Song, L., Al-Bassam, M.M., Bibb, M.J., and Challis, G.L. (2017)
897 Watasemycin biosynthesis in *Streptomyces venezuelae*: thiazoline C-methylation by a type B radical-SAM
898 methylase homologue. *Chem Sci* **8**: 2823–2831.
899
900 Jones, S.E., Ho, L.K., Rees, C.A., Hill, J.E., Nodwell, J.R., and Elliot, M.A. (2017) Streptomyces exploration
901 is triggered by fungal interactions and volatile signals. *eLife* **6**: e21738.
902
903 Keller, N.P. (2019) Fungal secondary metabolism: regulation, function and drug discovery. *Nat Rev*
904 *Microbiol* **17**: 167-180.
905
906 Kieser, T., Bibb, M.J., Buttner, M.J., Chater, K.F., and Hopwood, D.A. (2000) *Practical Streptomyces*
907 *Genetics*. The John Innes Foundation, Norwich, U.K.
908
909 Kurthkoti, K., Tare, P., Paitchowdhury, R., Gowthami, V.N., Garcia, M.J., Colangeli, R., *et al.* (2015) The
910 mycobacterial iron-dependent regulator IdeR induces ferritin (bfrB) by alleviating Lsr2 repression. *Mol*
911 *Microbiol* **98**: 864–877.
912
913 Lalaouna, D., Morissette, A., Carrier, M.C., and Massé, E. (2015) DsrA regulatory RNA represses both hns
914 and rbsD mRNAs through distinct mechanisms in *Escherichia coli*. *Mol Microbiol* **98**: 357–369.
915
916 Lang, A., Polnick, S., Nicke, T., William, P., Patallo, E.P., Naismith, J.H., and Pée, K.H. Van (2011) Changing
917 the regioselectivity of the tryptophan 7-halogenase PrnA by site-directed mutagenesis. *Angew Chemie -*
918 *Int Ed* **50**: 2951–2953.
919
920 Langmead, B., Trapnell, C., Pop, M., and Salzberg, S.L. (2009) Bowtie: An ultrafast memory-efficient short
921 read aligner. *Genome Biol* **10**: R25.
922
923 Larkin, M.A., Blackshields, G., Brown, N.P., Chenna, R., McGettigan, P.A., McWilliam, H., *et al.* (2007)
924 Clustal W and Clustal X version 2.0. *Bioinformatics* **23**: 2947–2948.
925
926 Li, H., Handsaker, B., Wysoker, A., Fennell, T., Ruan, J., Homer, N., *et al.* (2009) The Sequence Alignment
927 / Map format and SAMtools. *Bioinformatics* **25**: 2078–2079.
928
929 Lim, C.J., Lee, S.Y., Kenney, L.J., and Yan, J. (2012) Nucleoprotein filament formation is the structural
930 basis for bacterial protein H-NS gene silencing. *Sci Rep* **2**: 509.
931
932 Liu, G., Chater, K.F., Chandra, G., Niu, G., and Tan, H. (2013) Molecular regulation of antibiotic
933 biosynthesis in streptomyces. *Microbiol Mol Biol Rev* **77**: 112–43.
934
935 Liu, Y., Chen, H., Kenney, L.J., and Yan, J. (2010) A divalent switch drives H-NS/DNA-binding
936 conformations between stiffening and bridging modes. *Genes Dev* **24**: 339–344.
937
938 Livak, K.J., and Schmittgen, T.D. (2001) Analysis of relative gene expression data using real-time
939 quantitative PCR and the 2(-Delta Delta C(T)) method. *Methods* **25**: 402–408.
940
941 Lucchini, S., Rowley, G., Goldberg, M.D., Hurd, D., Harrison, M., and Hinton, J.C.D. (2006) H-NS mediates

- 942 the silencing of laterally acquired genes in bacteria. *PLoS Pathog* **2**: 0746–0752.
- 943
- 944 MacNeil, D.J., Gewain, K.M., Ruby, C.L., Dezeny, G., Gibbons, P.H., and MacNeil, T. (1992) Analysis of
945 *Streptomyces avermitilis* genes required for avermectin biosynthesis utilizing a novel integration vector.
946 *Gene* **111**: 61–68.
- 947
- 948 Mak, S., Xu, Y., and Nodwell, J.R. (2014) The expression of antibiotic resistance genes in antibiotic-
949 producing bacteria. *Mol Microbiol* **93**: 391–402.
- 950
- 951 Mann, H.B., and Whitney, D.R. (1947) On a test of whether one of 2 random variables is stochastically
952 larger than the other. *Ann Math Stat* **18**: 50–60.
- 953
- 954 Manteca, A., Ye, J., Sánchez, J., and Jensen, O.N. (2011) Phosphoproteome analysis of *Streptomyces*
955 development reveals extensive protein phosphorylation accompanying bacterial differentiation. *J*
956 *Proteome Res* **10**: 5481–5492.
- 957
- 958 McDonald, B.R., and Currie, C.R. (2017) Lateral gene transfer dynamics in the ancient bacterial genus
959 *Streptomyces*. *MBio* **8**: pii: e00644-17.
- 960
- 961 McKenzie, N.L., and Nodwell, J.R. (2007) Phosphorylated AbsA2 negatively regulates antibiotic
962 production in *Streptomyces coelicolor* through interactions with pathway-specific regulatory gene
963 promoters. *J Bacteriol* **189**: 5284–5292.
- 964
- 965 Moody, M.J., Young, R.A., Jones, S.E., and Elliot, M.A. (2013) Comparative analysis of non-coding RNAs in
966 the antibiotic-producing *Streptomyces* bacteria. *BMC Genomics* **14**: 558.
- 967
- 968 Müller, C.M., Schneider, G., Dobrindt, U., Emödy, L., Hacker, J., and Uhlin, B.E. (2010) Differential effects
969 and interactions of endogenous and horizontally acquired H-NS-like proteins in pathogenic *Escherichia*
970 *coli*. *Mol Microbiol* **75**: 280–293.
- 971
- 972 Najah, S., Saulnier, C., Pernodet, J.L., and Bury-Mone, S. (2019) Design of a generic CRISPR-Cas9
973 approach using the same sgRNA to perform gene editing at distinct loci. *BMC Biotechnol* **19**: 18.
- 974
- 975 Navarre, W.W. (2006) Selective silencing of foreign DNA with low GC content by the H-NS protein in
976 *Salmonella*. *Science* **313**: 236–238.
- 977
- 978 Navarre, W.W., McClelland, M., Libby, S.J., and Fang, F.C. (2007) Silencing of xenogeneic DNA by H-NS -
979 Facilitation of lateral gene transfer in bacteria by a defense system that recognizes foreign DNA. *Genes*
980 *Dev* **21**: 1456–1471.
- 981
- 982 Ochi, K., and Hosaka, T. (2013) New strategies for drug discovery: Activation of silent or weakly
983 expressed microbial gene clusters. *Appl Microbiol Biotechnol* **97**: 87–98.
- 984
- 985 Onaka, H. (2017) Novel antibiotic screening methods to awaken silent or cryptic secondary metabolic
986 pathways in actinomycetes. *J Antibiot* **70**: 865–870.
- 987
- 988 Paget, M.S.B., Chamberlin, L., Atrih, A., Foster, S.J., and Buttner, M.J. (1999) Evidence that the
989 extracytoplasmic function sigma factor σ^E is required for normal cell wall structure in *Streptomyces*

- 990 *coelicolor* A3(2). *J Bacteriol* **181**: 204–211.
991
992 Park, H.S., Östberg, Y., Johansson, J., Wagner, E.G.H., and Uhlin, B.E. (2010) Novel role for a bacterial
993 nucleoid protein in translation of mRNAs with suboptimal ribosome-binding sites. *Genes Dev* **24**: 1345–
994 1350.
995
996 Parker, J.L., Jones, A.M.E., Serazetdinova, L., Saalbach, G., Bibb, M.J., and Naldrett, M.J. (2010) Analysis
997 of the phosphoproteome of the multicellular bacterium *Streptomyces coelicolor* A3(2) by
998 protein/peptide fractionation, phosphopeptide enrichment and high-accuracy mass spectrometry.
999 *Proteomics* **10**: 2486–2497.
1000
1001 Peirson, S.N. (2003) Experimental validation of novel and conventional approaches to quantitative real-
1002 time PCR data analysis. *Nucleic Acids Res* **31**: e73.
1003
1004 Petkau, A., Stuart-Edwards, M., Stothard, P., and Domselaar, G. van (2010) Interactive microbial genome
1005 visualization with GView. *Bioinformatics* **26**: 3125–3126.
1006
1007 Pfannenstiel, B.T., and Keller, N.P. (2019) On top of biosynthetic gene clusters: How epigenetic
1008 machinery influences secondary metabolism in fungi. *Biotechnol Adv* pii: S0734-9750(19)30012-6.
1009
1010 Pluskal, T., Castillo, S., Villar-Briones, A., and Oresic, M. (2010) MZmine 2: modular framework for
1011 processing, visualizing, and analyzing mass spectrometry-based molecular profile data. *BMC*
1012 *Bioinformatics* **11**: 395.
1013
1014 Rigali, S., Titgemeyer, F., Barends, S., Mulder, S., Thomae, A.W., Hopwood, D.A., and Wezel, G.P. van
1015 (2008) Feast or famine: the global regulator DasR links nutrient stress to antibiotic production by
1016 *Streptomyces*. *EMBO Rep* **9**: 670–675.
1017
1018 Robinson, J.T., Thorvaldsdóttir, H., Winckler, W., Guttman, M., Lander, E.S., Getz, G., and Mesirov, J.P.
1019 (2011) Integrative genomics viewer. *Nat Biotechnol* **29**: 24–26.
1020
1021 Ryan Will, W., Whitham, P.J., Reid, P.J., and Fang, F.C. (2018) Modulation of H-NS transcriptional
1022 silencing by magnesium. *Nucleic Acids Res* **46**: 5717–5725.
1023
1024 Salerno, P., Larsson, J., Bucca, G., Laing, E., Smith, C.P., and Flärdh, K. (2009) One of the two genes
1025 encoding nucleoid-associated HU proteins in *Streptomyces coelicolor* is developmentally regulated and
1026 specifically involved in spore maturation. *J Bacteriol* **191**: 6489–6500.
1027
1028 Scharf, D.H., and Brakhage, A.A. (2013) Engineering fungal secondary metabolism: A roadmap to novel
1029 compounds. *J Biotechnol* **163**: 179–183.
1030
1031 Schmieder, R., and Edwards, R. (2011) Quality control and preprocessing of metagenomic datasets.
1032 *Bioinformatics* **27**: 863–864.
1033
1034 Singh, S.S., Singh, N., Bonocora, R.P., Fitzgerald, D.M., Wade, J.T., and Grainger, D.C. (2014) Widespread
1035 suppression of intragenic transcription initiation by H-NS. *Genes Dev* **28**: 214–219.
1036
1037 Smith, C.A., Want, E.J., O’Maille, G., Abagyan, R., and Siuzdak, G. (2006) XCMS: Processing mass

- 1038 spectrometry data for metabolite profiling using nonlinear peak alignment, matching, and identification.
1039 *Anal Chem* **78**: 779–787.
- 1040
- 1041 Smits, W.K., and Grossman, A.D. (2010) The transcriptional regulator Rok binds A+T-rich DNA and is
1042 involved in repression of a mobile genetic element in *Bacillus subtilis*. *PLOS Genet* **6**: e1001207.
- 1043
- 1044 Stark, R., and Brown, G. (2011) *DiffBind*: differential binding analysis of ChIP-Seq peak data.
1045 <https://bioconductor.org/packages/release/bioc/html/DiffBind.html>.
- 1046
- 1047 Swiercz, J.P., Nanji, T., Gloyd, M., Guarné, A., and Elliot, M.A. (2013) A novel nucleoid-associated protein
1048 specific to the actinobacteria. *Nucleic Acids Res* **41**.
- 1049
- 1050 Team, R.C. (2013) R: A language and environment for statistical computing. <http://www.r-project.org/>.
- 1051
- 1052 La Teana, A., Brandi, A., Falconi, M., Spurio, R., Pon, C.L., and Gualerzi, C.O. (2006) Identification of a
1053 cold shock transcriptional enhancer of the *Escherichia coli* gene encoding nucleoid protein H-NS. *Proc*
1054 *Natl Acad Sci* **88**: 10907–10911.
- 1055
- 1056 Thaker, M.N., Wang, W., Spanogiannopoulos, P., Waglechner, N., King, A.M., Medina, R., and Wright,
1057 G.D. (2013) Identifying producers of antibacterial compounds by screening for antibiotic resistance. *Nat*
1058 *Biotechnol* **31**: 922–927.
- 1059
- 1060 Thanapipatsiri, A., Gomez-Escribano, J.P., Song, L., Bibb, M.J., Al-Bassam, M., Chandra, G., *et al.* (2016)
1061 Discovery of unusual biaryl polyketides by activation of a silent *Streptomyces venezuelae* biosynthetic
1062 gene cluster. *ChemBioChem* **17**: 2189–2198.
- 1063
- 1064 Tjaden, B. (2015) De novo assembly of bacterial transcriptomes from RNA-seq data. *Genome Biol* **16**: 1.
- 1065
- 1066 Valk, R.A. van der, Vreede, J., Qin, L., Moolenaar, G.F., Hofmann, A., Goosen, N., and Dame, R.T. (2017)
1067 Mechanism of environmentally driven conformational changes that modulate H-NS DNA-bridging
1068 activity. *eLife* **6**: pii: e27369.
- 1069
- 1070 Wang, R., Mast, Y., Wang, J., Zhang, W., Zhao, G., Wohleben, W., *et al.* (2013) Identification of two-
1071 component system AfsQ1/Q2 regulon and its cross-regulation with GlnR in *Streptomyces coelicolor*. *Mol*
1072 *Microbiol* **87**: 30–48.
- 1073
- 1074 Wezel, G.P. van, and McDowall, K.J. (2011) The regulation of the secondary metabolism of
1075 *Streptomyces*: new links and experimental advances. *Nat Prod Rep* **28**: 1311–1333.
- 1076
- 1077 Will, W.R., Navarre, W.W., and Fang, F.C. (2015) Integrated circuits: How transcriptional silencing and
1078 counter-silencing facilitate bacterial evolution. *Curr Opin Microbiol* **8**–13.
- 1079
- 1080 Williamson, N.R., Fineran, P.C., Leeper, F.J., and Salmond, G.P.C. (2006) The biosynthesis and regulation
1081 of bacterial prodiginines. *Nat Rev Microbiol* **4**: 887–899.
- 1082
- 1083 Yoon, V., and Nodwell, J.R. (2014) Activating secondary metabolism with stress and chemicals. *J Ind*
1084 *Microbiol Biotechnol* **41**: 415–424.
- 1085

- 1086 Zhang, Y., Liu, T., Meyer, C.A., Eeckhoute, J., Johnson, D.S., Bernstein, B.E., *et al.* (2008) Model-based
1087 analysis of CHIP-seq (MACS). *Genome Biol* **9**: R137.
1088
1089 Ziemert, N., Lechner, A., Wietz, M., Millan-Aguinaga, N., Chavarria, K.L., and Jensen, P.R. (2014) Diversity
1090 and evolution of secondary metabolism in the marine actinomycete genus *Salinispora*. *Proc Natl Acad*
1091 *Sci* **111**: E1130–E1139.
1092

1093 **Table 1. Specialized metabolic clusters and their control by Lsr2**

Predicted specialized metabolic gene cluster# (characterized product)	1st gene	Last gene	Number of upregulated genes (<i>q</i> -value <0.01; >4 fold change)	% of upregulated genes in each cluster	Number of Lsr2-associated sites (<i>q</i> -value <0.01)
Ectoine	SVEN_0223	SVEN_0234	1	8.33	0
Terpene	SVEN_0261	SVEN_0306	1	0	0
T1PKS-T3PKS-NRPS (venemycin/watasemycin/ thiazostatin)	SVEN_0463	SVEN_0531	28	42.65	2 (SVEN_0502*, 506)
Lantipeptide – terpene	SVEN_0540	SVEN_0561	0	0	1 (SVEN_0557)
Lantipeptide (<i>venezuelin</i>)	SVEN_0612	SVEN_0630	3 (1 repressed)	16.67	0
Indole (<i>acryriaflavin</i>)	SVEN_0755	SVEN_0772	0	0	0
Chloramphenicol	SVEN_0913	SVEN_0928	14	93.33	1 (SVEN_0926)
Other	SVEN_1844	SVEN_1884	0	0	0
Siderophore (desferrioxamine-like)	SVEN_2566	SVEN_2577	5	41.67	1 (SVEN_2576)
Lasso peptide	SVEN_3103	SVEN_3132	2	6.90	1 (SVEN_3116*-7)
Other	SVEN_4061	SVEN_4110	1	2.04	1 (SVEN_4069-70)
Butyrolactone (<i>gaburedin</i>)	SVEN_4179	SVEN_4189	0	0	0
Melanin	SVEN_4620	SVEN_4662	0	0	4 (SVEN_4629-30, 4632, 4634-5, 4651)
Butyrolactone	SVEN_5076	SVEN_5111	3	11.54	2 (SVEN_5091-92, 5106*-07)
Thiopeptide	SVEN_5119	SVEN_5145	3	11.54	3 (SVEN_5127-8, 5129-31, 5132-3)
T3pks	SVEN_5351	SVEN_5383	0	0	0
Siderophore	SVEN_5413	SVEN_5426	0	0	0
Siderophore	SVEN_5471	SVEN_5482	(1 repressed)	9.09	0
Bacteriocin	SVEN_5817	SVEN_5840	3	15.15	1 (SVEN_5817*)
Butyrolactone – T2PKS	SVEN_5951	SVEN_6002	19	45.10	6 (SVEN_5963*-4, 5968*-9, 5972-3, 5974, 5975-6, 5979)
Other	SVEN_6112	SVEN_6204	3 (1 repressed)	3.26	1 (SVEN_6199)
NRPS-ladderane	SVEN_6134	SVEN_6282	50	36.49	7 (SVEN_6199, 6216-7, 6219-20, 6225*, 6230, 6247-8, 6251)
Terpene	SVEN_6436	SVEN_6490	6	16.67	1 (SVEN_6458)
Bacteriocin	SVEN_6527	SVEN_6535	(1 repressed)	0	0
T2PKS	SVEN_6767	SVEN_6814	2	4.26	0
Melanin	SVEN_6833	SVEN_6842	4	44.44	0
NRPS	SVEN_7032	SVEN_7080	0	0	0
Terpene	SVEN_7101	SVEN_7119	(2 repressed)	0	1 (SVEN_7109-10*)
T3PKS	SVEN_7223	SVEN_7259	1	2.78	2 (SVEN_7235, 7237*-8)
Terpene-NRPS	SVEN_7417	SVEN_7452	0	0	4 (SVEN_7427-8, 7440, 7447-9, 7449-50)

1094 #: Cluster prediction by antiSMASH; * Asterisks indicate regulatory genes bound by Lsr2

1095 **Bold: clusters containing an Lsr2 binding site**

1096 *Grey shading: clusters containing differentially expressed genes*

1097 **FIGURE LEGENDS**

1098

1099 **Figure 1. Expression and phenotypic analyses of *lsr2* and *lsrL* in *S. venezuelae*.**

1100 **(A)** Growth curves and developmental stages (as determined using light microscopy) of wild type (WT),
1101 and the three different *lsr2/lsrL* mutants, over a 40 h time course in MYM liquid medium.

1102 **(B)** Comparing development (left) and melanin/brown pigment production (right – underside of plate) of
1103 wild type (WT), versus single (Δ *lsr2* and Δ *lsrL*) and double (Δ *lsr2* Δ *lsrL*) mutant strains after 2 d growth on
1104 MYM agar medium. The white colour of the *lsr2*-containing mutants reflects aerial hyphae formation,
1105 while the darker colour associated with the wild type and *lsrL* mutant strains indicates culture
1106 sporulation.

1107 **(C)** Comparative transcript levels (RPKM = reads per kilobase per million) for *lsr2* and *lsrL* at three time
1108 points [T1, T2, T3, representing the three developmental stages indicated in (A)] in liquid MYM medium,
1109 as assessed using RNA-sequencing data. Data are presented as mean \pm standard deviation ($n = 2$).

1110

1111 **Figure 2. Composition of *S. venezuelae* chromosome in relation to Lsr2 binding sites and differentially**
1112 **affected genes.**

1113 **(A)** Panels are described from the bottom up. Bottom panels: coding sequences and relative strand
1114 organization (forward orientation shown in red; reverse orientation shown in blue) across the *S.*
1115 *venezuelae* chromosome, with left arm, core and right arm regions indicated. Above that, the regions
1116 shown with black bars indicate the relative position of predicted phage genes, while those in yellow
1117 indicate the location of specialized metabolic clusters. The light blue bars represent genes whose
1118 expression is significantly upregulated in the *lsr2* mutant (fold change indicated), while the pink bars
1119 indicate Lsr2 binding sites, as determined by ChIP-seq. The top panel depicts the GC content of the
1120 chromosome, relative to the average percentage (72.4%). The peaks above the middle line indicate a GC
1121 content above 72.4%, while those below indicate a GC content below 72.4%. Image was generated using
1122 GView (Petkau *et al.*, 2010).

1123 **(B)** Binding sites within the left arm (pink), core (green) or right arm (blue), and relative proportion of
1124 sites associated with transcriptional changes (no change in transcription=darker colour; change in
1125 transcription=lighter colour). Shown within each segment is the number of binding sites associated with
1126 that region.

1127 **(C)** Size of binding sites (in base pairs, bp) in each of the chromosome regions, separated into those
1128 associated with altered transcription (change), versus not (no change). Colour scheme is as described in
1129 (B). The average binding site size for each group is indicated by the vertical black line.

1130
1131 **Figure 3. Lsr2 binding sites and expression analysis of select Lsr2-regulated specialized metabolic**
1132 **clusters.** For each of the six specialized metabolic clusters shown, genes oriented in the forward
1133 direction are shown as pink boxes, while those in the reverse direction are shown as blue boxes. Select
1134 genes are labelled with their corresponding *sven* numbers (e.g. 0481). RNA-sequencing results are
1135 shown above each cluster, with graphs depicting expression levels. For each, the *Lsr2* read profile is
1136 shown on the top, while the wild type profile is shown on the bottom. The ChIP-seq profiles (below the
1137 gene cluster) are shown as 'fold increase', with the grey profiles indicating regions associated with
1138 3×FLAG-tagged Lsr2 (where an anti-FLAG antibody was used for the immunoprecipitation), and the black
1139 profile representing the negative control (strain expressing a non-FLAG-tagged Lsr2 variant). Lsr2-
1140 3×FLAG binding sites are indicated with a red asterisk.

1141
1142 **Figure 4. Conservation of specialized metabolic clusters in diverse streptomycetes.** Phylogenetic tree
1143 of diverse *Streptomyces* species, with the relative conservation of each specialized metabolic cluster
1144 from *S. venezuelae* shown in the right. Conservation is based on BLAST analyses, with <20% (white), 20%
1145 (light pink), 40% (medium pink) and 60% (dark pink) indicating query coverage and overall degree of
1146 cluster conservation. Clusters bound by Lsr2 are indicated with bolded names and solid circles, while
1147 those not bound by Lsr2 are depicted with dotted circles.

1148
1149 **Figure 5. Specialized and volatile metabolite comparisons between wild type and *Lsr2* mutant strains.**
1150 **(A)** Bioactivity of *S. venezuelae* extracts against *Micrococcus luteus*. Wild type and *Lsr2* mutant strains
1151 were cultured for 18 h prior to extraction in methanol and reconstitution in DMSO. Extracts were
1152 applied to Whatman filter discs, alongside a chloramphenicol positive control.
1153 **(B)** Extracted ion chromatogram for chloramphenicol (m/z 321.005), from LC/MS analysis of methanol
1154 extracts from wild type and *Lsr2* mutant cultures grown in MYM liquid medium for 3 d, alongside a
1155 medium (MYM) control.
1156 **(C)** Extracted ion chromatograms of $[M-H]^- = 219.040$ (venemycin); $[M-H]^- = 252.992$ (chlorinated
1157 venemycin); $[M + H]^+ = 353.099$ (watasemycin); and $[M + H]^+ = 339.083$ (thiazostatin), from LC/MS
1158 analyses of methanol extracts of wild type and *Lsr2* mutant strains grown for 3 d in MYM liquid medium.
1159 **(D)** Extracted ion chromatogram of m/z 281.068, from LC/MS analysis of methanol extracts of wild type,
1160 *Lsr2* mutant and double *Lsr2 sven_6229* mutant strains, grown in MYM liquid medium for 3 d.

1161 **(E)** Heat map depicting the 65 volatile compounds (columns) that were significantly different in relative
1162 abundance ($p < 0.05$ after BH correction) between wild type (WT, red) and *lsr2* mutant (Δ *lsr2*, blue)
1163 strains. Sterile media (Media, green) is included for comparison. Cell color corresponds to relative
1164 compound abundance after \log_{10} -transformation, mean-centering, and unit-scaling, ranging from low
1165 abundance (blue) to high abundance (red). Dendrogram (left) was constructed using Euclidean distance
1166 as the distance metric.

1167

1168 **Figure 6. Manipulating Lsr2 activity can stimulate new antibiotic production in diverse *Streptomyces*.**

1169 **(A)** Lsr2 activity ‘knockdown’ construct, where a DNA-binding defective variant of Lsr2 (*lsr2**) is under
1170 the control of a constitutive (*ermE**) promoter, and is on a plasmid vector bearing an apramycin
1171 resistance marker, that is capable of integrating into the chromosomes of most, if not all,
1172 streptomycetes.

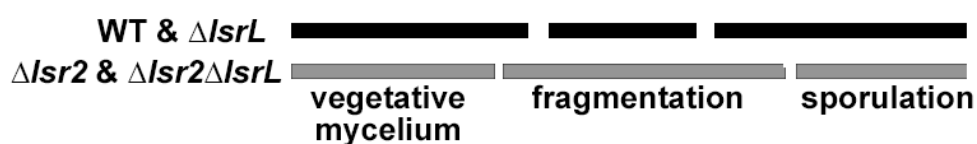
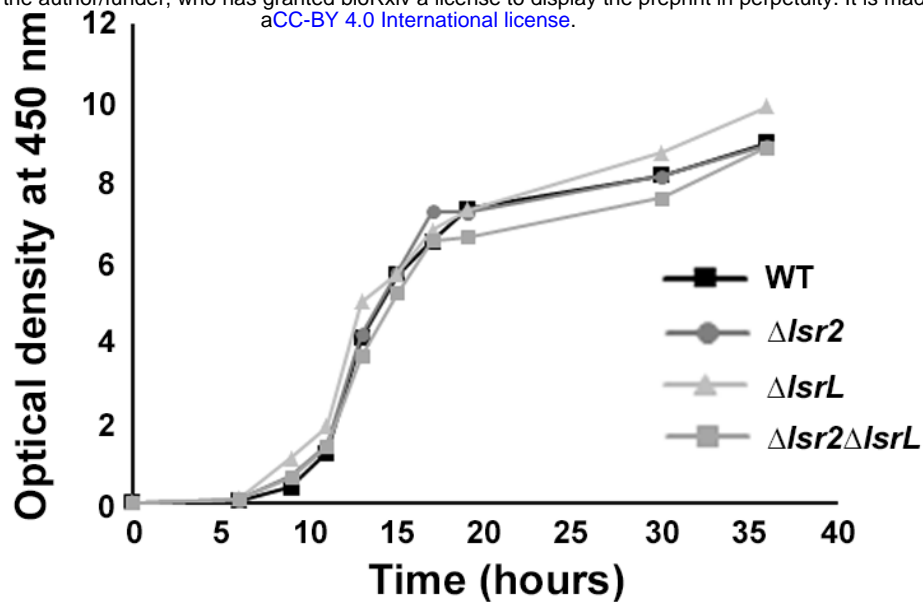
1173 **(B)** Growth of *Streptomyces coelicolor* on Difco nutrient agar. Top left, wild type; top right: wild type
1174 carrying the empty plasmid; bottom: replicates of wild type carrying the plasmid with dominant negative
1175 *lsr2** variant.

1176 **(C)** Antibiotic bioassay using the wild *Streptomyces* strain WAC4718, bearing either the control (empty)
1177 plasmid (C), or the Lsr2 knockdown construct (*), tested against the indicator strains *M. luteus* (MI) or
1178 *Bacillus subtilis* (Bs). Error bars indicate standard error ($n=4$).

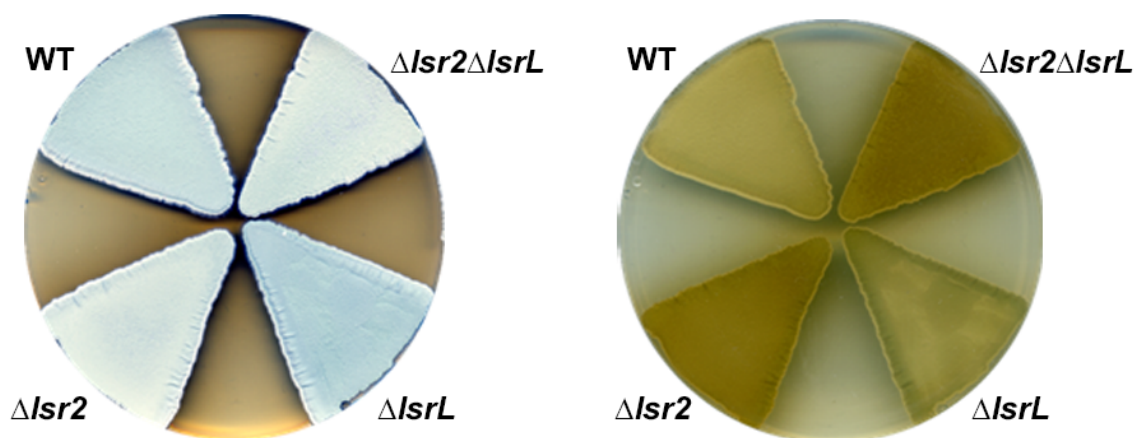
1179 **(D)** Antibiotic bioassay using four different wild *Streptomyces* strains (WAC5514, WAC6377, WAC7072,
1180 and WAC7520), carrying either empty plasmid (C) or the Lsr2 knockdown construct (*), tested against *M.*
1181 *luteus* as an indicator strain. Error bars indicate standard error ($n=4$).

1182

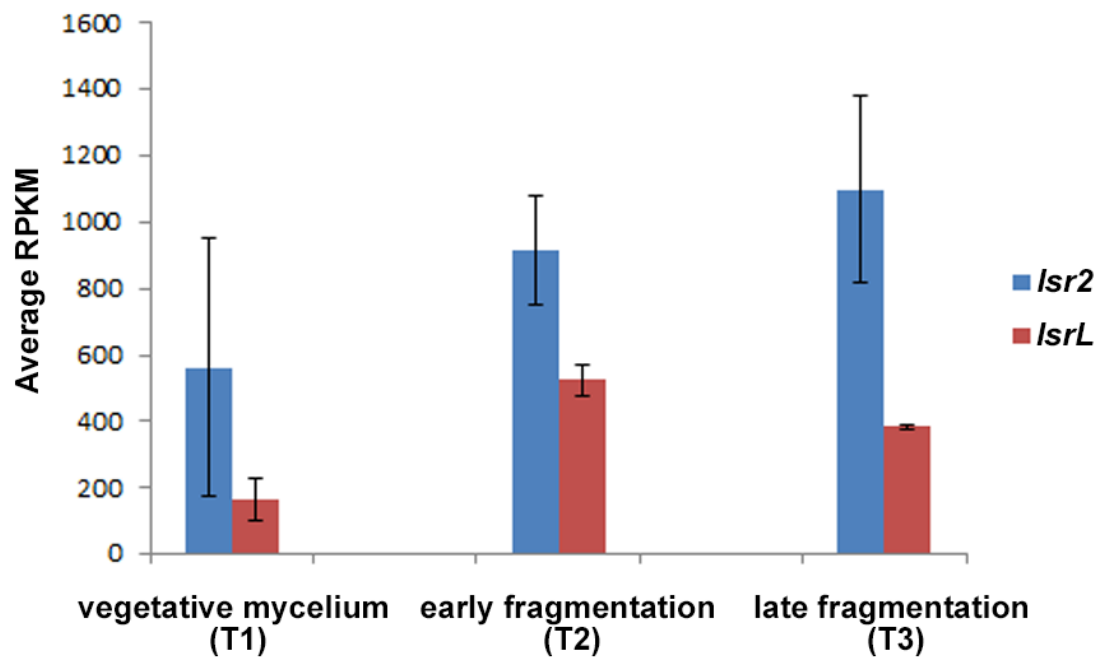
A

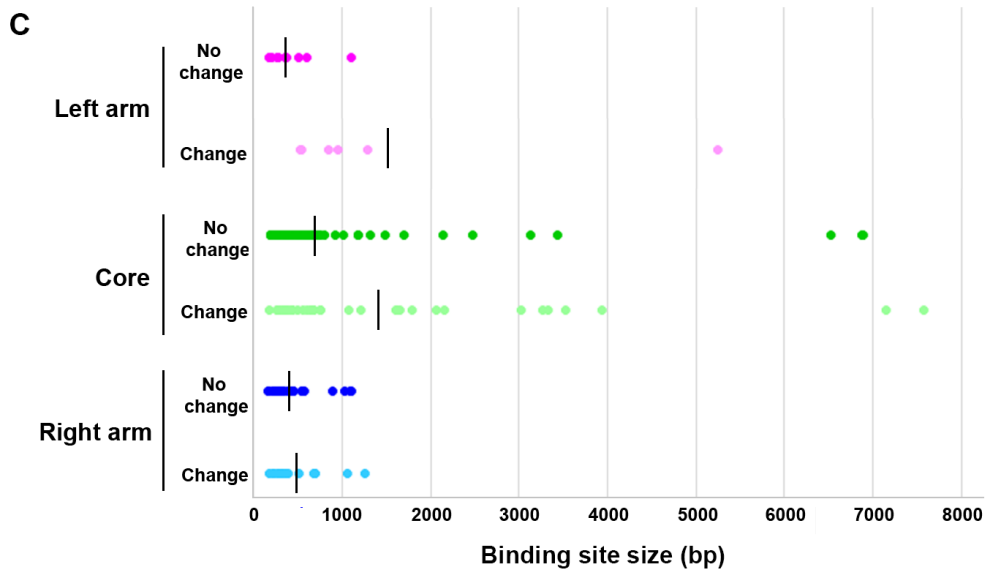
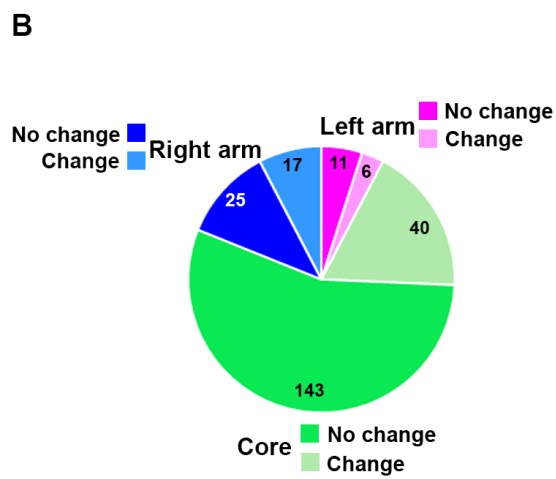
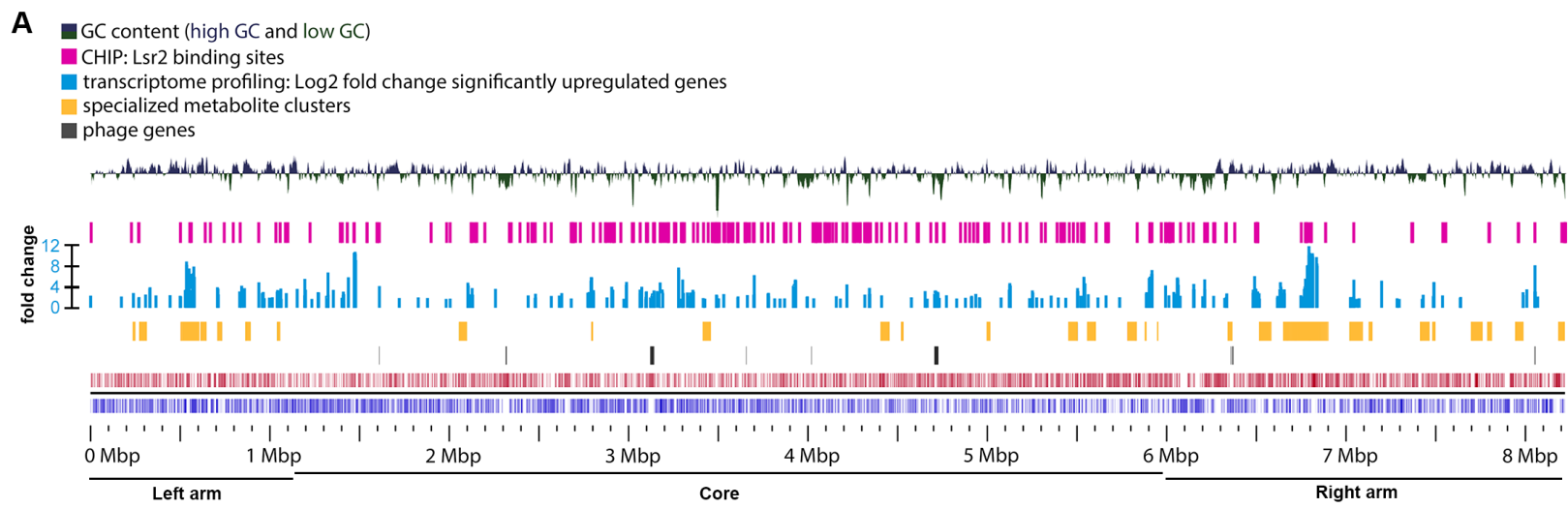


B

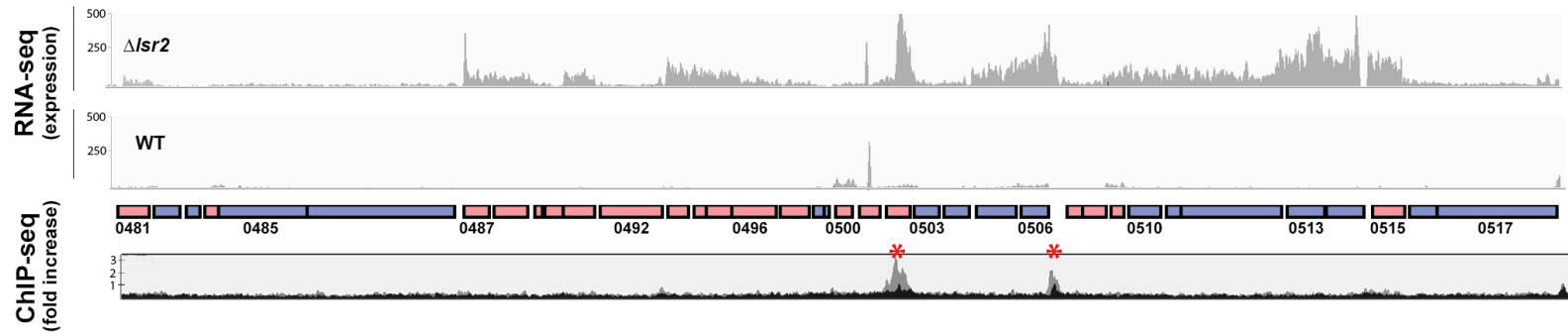


C

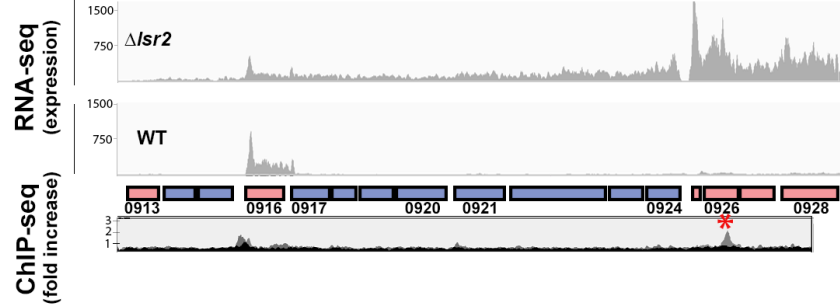




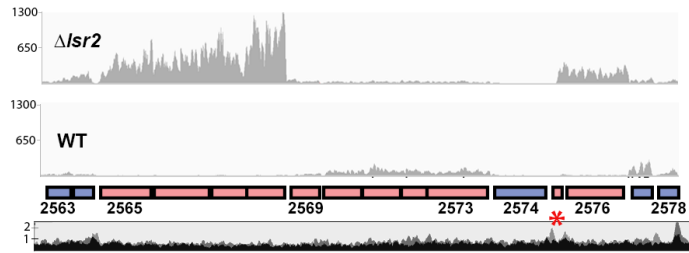
Type I PKS/Type 3 PKS/NRPS



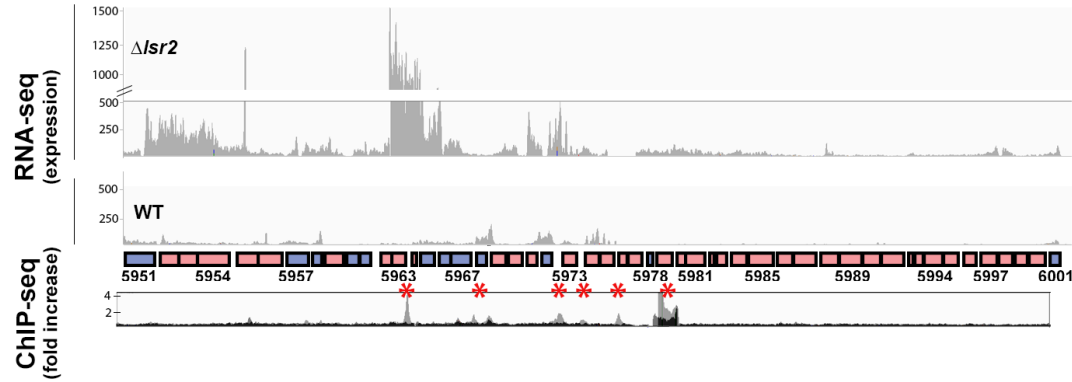
Chloramphenicol



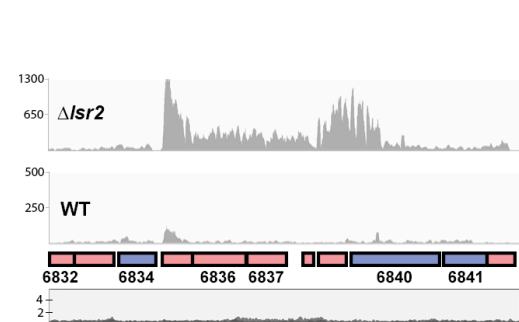
Siderophore



NRPS



Melanin



NRPS-ladderane

